Magnesium cationic cue enriched interfacial tissue microenvironment nurtures the osseointegration of gamma-irradiated allograft bone

Wenhao Wang [a,b,c,d,1], Jie Shen [b,c,e,1], Yuan Meng [a,d,1], Miaoman Ye [a], Shaozhang Lin [a], Qi Zhao [a], Le Wang [a,d], Kenneth M.C. Cheung [b,c], Shuilin Wu [f,g], Yufeng Zheng [h], Xuanyong Liu [i], Paul K. Chu [j], Kelvin W.K. Yeung [b,c,**], Zhi-Yong Zhang [a,d,*]

[a] Translational Research Centre of Regenerative Medicine and 3D Printing of Guangzhou Medical University, Guangdong Province Engineering Research Center for Biomedical Engineering, State Key Laboratory of Respiratory Disease, The Third Affiliated Hospital of Guangzhou Medical University, Guangzhou, 510150, PR China
[b] Department of Orthopaedics and Traumatology, The University of Hong Kong, Hong Kong, 999077, PR China
[c] Shenzhen Key Laboratory for Innovative Technology in Orthopaedic Trauma, The University of Hong Kong Shenzhen Hospital, Shenzhen, 518053, PR China
[d] Department of Orthopaedic Surgery, The Third Affiliated Hospital of Guangzhou Medical University, Guangzhou, 510150, PR China
[e] Shenzhen Key Laboratory of Spine Surgery, Department of Spine Surgery, Peking University Shenzhen Hospital, Shenzhen, 518036, PR China
[f] Ministry of Education Key Laboratory for the Green Preparation and Application of Functional Materials, Hubei Key Laboratory of Polymer Materials, School of Materials & Engineering, Hubei University, Wuhan, 430062, PR China
[g] Ministry of Education Key Laboratory for Advanced Ceramics and Machining Technology, School of Materials Science & Engineering, Tianjin University, Tianjin, 300352, PR China
[h] State Key Laboratory for Turbulence and Complex System, Department of Materials Science and Engineering, Collage of Engineering, Peking University, Beijing, 100871, PR China
[i] State Key Laboratory of High Performance Ceramics and Superfine Microstructure, Shanghai Institute of Ceramics, Chinese Academy of Sciences, Shanghai, 200050, PR China
[j] Department of Materials Science and Engineering, City University of Hong Kong, Hong Kong, 999077, PR China

ARTICLE INFO

ABSTRACT

Regardless of the advancement of synthetic bone substitutes, allograft-derived bone substitutes still dominate in the orthopaedic circle in the treatments of bone diseases. Nevertheless, the stringent devitalization process jeopardizes their osseointegration with host bone and therefore prone to long-term failure. Hence, improving osseointegration and transplantation efficiency remains important. The alteration of bone tissue microenvironment (TME) to facilitate osseointegration has been generally recognized. However, the concept of exerting metal ionic cue in bone TME without compromising the mechanical properties of bone allograft is challenging. To address this concern, an interfacial tissue microenvironment with magnesium cationc cue was tailored onto the gamma-irradiated allograft bone using a customized magnesium-plasma surface treatment. The formation of the Mg cationic cue enriched interfacial tissue microenvironment on allograft bone was verified by the scanning ion-selective electrode technique. The cellular activities of human TERT-immortalized mesenchymal stem cells on the Mg-enriched grafts were notably upregulated. In the animal test, superior osseointegration between Mg-enriched graft and host bone was found, whereas poor integration was observed in the gamma-irradiated controls at 28 days post-operation. Furthermore, the bony in-growth appeared on magnesium-enriched allograft bone was significant higher. The mechanism possibly correlates to the up-regulation of integrin receptors in mesenchymal stem cells under modified bone TME that directly orchestrate the initial cell attachment and osteogenic differentiation of mesenchymal stem cells. Lastly, our findings demonstrate the significance of magnesium cation modified bone allograft that can potentially translate to various orthopaedic procedures requiring bone augmentation.

1. Introduction

Bone grafting is highly recommended for the treatment of segmental bone loss caused by multifragmental traumatic injuries [1], bone tumor excisions [2], or disc degeneration due to aging [3]. In fact, the bone graft is the second most common type of transplant tissue only after blood [4], and the inadequate supply makes them far from satisfying the clinical demands [5], leading to the rapid development of regenerative medicine. Nevertheless, strategies utilized to address bone regeneration have historically relied on the incorporation of biological supplements, such as functional cells and bioactive factors [6]. More recently, with the emergence of advances in biomaterials and the profound understanding of the complexities of the cell-biomaterial interactions [7], it is increasingly clear that the tissue microenvironment, which is composed of regenerative signals and cues that characteristically attributed to the materials in the cellular microenvironment, substantially influences the cellular behaviors and thus determines the osseointegration responding to bone material implants [7,8]. Unfortunately, the abundance of the regenerative niche, which is inherently accumulated in the natural tissue substitutes, is rare within the interfacial tissue microenvironment conferred by synthetic options and thus leading to the jeopardized clinical application [9]. As a result, allograft bone remains the most commonly used graft in number of clinical orthopaedic scenarios [10].

Allograft bone can be manufactured into a variety of shapes together with inherent structural integrity and inherent regenerative niche. However, the stringent processing and compulsory terminal sterilization (e.g. gamma irradiation) impair the clinical outcomes of allograft bone transplantation in terms of fibrotic tissue encapsulation and slower integration [11], thereby leading to the higher risk of secondary fracture compared the non-irradiated allograft bone [12,13]. To improve the transplantation efficiency and translational potency in clinics, a well-established approach to rescue the osseointegration of allograft bone is to modify its surface that leads to alter its interfacial tissue microenvironment. As a well-orchestrated process, attachment of osteoprogenitor cells, osteogenic differentiation, and the subsequent osseointegration of the implant are always initiated with the cell-material interactions in the interfacial tissue microenvironment [14]. The interfacial biophysical and biochemical properties, especially the nanotopography [15], stiffness [16], and chemical cues [17], have also been found to play key roles in stem cell fate decision, which is directly associated with the osseointegration and transplantation efficiency of implants [7]. Indeed, given the diversity of the material properties, the developments in the past few years have advanced the hypothesis that controlling the interfacial tissue microenvironment usually demonstrates convincing osseointegration while maintaining the controllability and feasibility, and the side effect is rare [18]. Nevertheless, harsh machining is not recommended for allograft bone in consideration of the embrittlement after the gamma-irradiated sterilization, which directly leads to higher incidence of secondary fracture [19].

Multiscale investigations have revealed that magnesium (Mg), one of the most abundant bioinorganic cations in the human body, is a convincing regenerative cue, especially when bone tissue environment contains suitable concentration of Mg ions [20,21]. Nevertheless, the concept of exerting a magnesium cationic cue enriched interfacial tissue microenvironment on bone allograft directly is rare. Traditional protocols used to establish such kind of interfacial tissue microenvironment rely on the incorporation of hydrogel containing magnesium. Due to the complexity of cancellous bone structure, the bioinorganic cations or biochemical cue contained hydrogel may not be able to penetrate into the internal construction thoroughly. Alternatively, someone proposed to submerge the bone graft with magnesium or strontium containing solution [22–24]. However, this approach was unable to establish a controlled cation release profile and therefore burst release would likely happen. To address these uncertainties, we have adopted a surface treatment technique, namely plasma immersion ion implantation and deposition, to exert a layer of Mg that can manipulate a programmable release of magnesium cations in bone tissue microenvironment. Because of the mobility of Mg plasma, an intensive penetration of magnesium over entire cancellous structure can be therefore expected. The formation of an Mg^{2+}-cue enriched interfacial tissue microenvironment on bone allograft was verified using the scanning ion-selective electrode technique (SIET). The cell spreading, proliferation, osteogenic differentiation, and mineralization of human TERT-immortalized mesenchymal stem cells (hTMSCs) on Mg^{2+}-cue enriched samples were also assayed. The *in vivo* osseointegration between host bone and allograft bone was demonstrated in rat model, and the underlying mechanism was explored through antibody-blocking and RNA interference experiments.

2. Materials and methods

2.1. Decellularized bone graft preparation and characterizations

The cortical and cancellous bone slices measured in 1 mm thick (10*10*1 mm) were harvested from the fresh bovine femora purchased in Hong Kong. All the articular cartilage and soft tissue were removed by a precision saw system (EXAKT 300cp Band System, EXAKT, Germany), and elimination of bone marrow and decellularization process were performed according to a published protocol [25] (Fig. 1a). Briefly, a high-pressure water jet (Pulsavac Plus, Zimmer, USA) was used to wash the cancellous bone slices with physiological saline (B. Braun Melsungen, Malaysia) until most of the tissue, including bone marrow and adipose tissue, was removed. The porous and dense bone slices were then immersed in a 5% $NaHCO_3$ (Sigma-Aldrich, USA) aqueous solution at 50 °C for 24 h, and the non-mineralized organic components were completely hydrolyzed and removed [26]. Afterwards, the slices were extensively defatted in two baths of absolute acetone (8 h for each bath), followed by two baths of 40% ethanol (4 h for each bath) after three washes with distilled water. The decellularized bovine bone slices were finally dried in an oven at 37 °C until a stable weight was obtained and cut into small pieces (10*10*1 mm) before storing in sterilized bags. In order to obtain the interfacial properties, the nonporous cortical bone slices would be used for X-ray photoelectron spectroscopy (XPS) and interfacial Mg^{2+} cationic microenvironment analysis, while the cancellous bone slices would be used for other characterizations and *in vitro* investigations.

Additionally, the allograft bone collected from the carcasses of Sprague-Dawley (SD) rats weighing about 250–350g (provided by the Laboratory Animal Unit of the University of Hong Kong) were applied for *in vivo* analysis. The samples measured in 6 mm long and 2 mm in diameter were harvested from femoral and the soft tissue was eliminated and followed by the decellularization process as previously described. After drying in a vacuum oven, the decellularized allogeneic bone rods were stored in sterilized bags.

Samples of graft materials from each group were then fixed, dehydrated and embedded by PMMA resin before sectioning and staining by Giemsa-Eosin. Visualized images were obtained using light microscopy (Nikon Eclipse 80i, Japan). Furthermore, the structural integrity of the decellularized and plasma surface treated bone matrix were examined using scanning electron microscopy (SEM, Hitachi S-4800 FEG SEM, Japan) and the nano-indenter (Nano Indenter G200, USA), respectively.

2.2. Surface tailoring of the decellularized bone graft

Two steps were involved in the preparation of the magnesium cationic cue enriched decellularized bone slices. Firstly, a transitional layer was prepared by the magnesium plasma immersion ion implantation (PIII) process. Consequently, the magnesium-coating layer was deposited on top of the transitional layer with the automated multipurpose plasma processing system at a nitrogen flow rate of 25sccm. A pulsed voltage of 300 V and pulsing frequency of 50 Hz were applied.

The detailed parameters were listed in Table 1. All magnesium-treated samples and control bone slices were then sterilized by gamma irradiation at a dose of 30 KGy.

2.3. Characterizations of magnesium-treated decellularized bone graft

2.3.1. Surface morphology

The surface morphology of the control and magnesium-treated decellularized cancellous bone matrix was observed via SEM. The collagen-like and microporous structures were screened under higher magnification.

2.3.2. Surface elemental composition and magnesium depth profile

The magnesium-treated cortical bone slices were used for this test. The full elemental compositions of the Mg-treated surfaces were obtained via X-ray photoelectron spectroscopy (XPS) with the employment of Al K$_\alpha$ irradiation, and all binding energies were referenced to the C 1s line at 285.0 eV. The implantation depth profiles of magnesium were then obtained with an estimated sputtering rate of 34.13 nm/min.

The surface chemical composition and the magnesium elemental

Table 1
Parameters for plasma immersion ion implantation and deposition (PIII&D).

	1st Process-Mg Implantation	2nd Process-Mg Deposition
Ar Flow Speed	25sccm	25sccm
Working Pressure	8.5×10^{-2}Pa	9×10^{-2}Pa
Voltage	20 KV (200μs,6Hz)	300 V (DC)
Current	9 mA	20 mA
Implantation Time	1 h	–
Deposition Time	–	1 h (Mg-enriched (1hr)) & 4 h (Mg-enriched (4hr))

mapping were determined by energy-dispersive x-ray spectroscopy (EDS).

2.3.3. Detection of the interfacial and spatiotemporal magnesium microenvironment

Scanning ion-selective electrode technique (SIET), after slightly adjusting based on previously reported literature [27], was applied (Xuyue Sci. and Tech. Co., Ltd., China) to monitor the alteration of interfacial tissue microenvironment in terms of the Mg cation cue
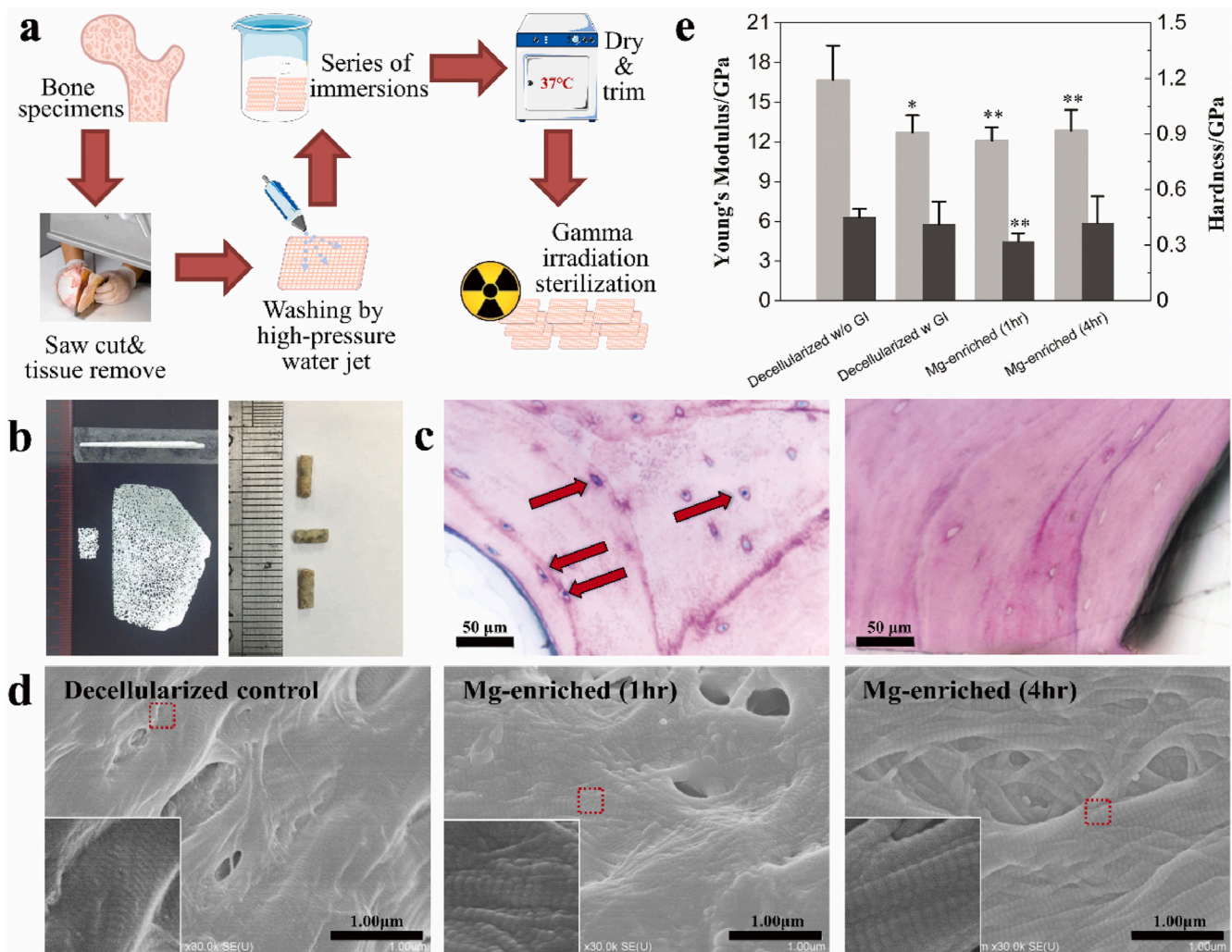
Fig. 1. Preparation and characterizations of the decellularized control, Mg-enriched (1hr) and Mg-enriched (4hr) samples. (a) Scheme of the allograft bone processing and (b) the morphological examination of the decellularized bovine bone slice and rat allograft bone. (c) Visualization of decellularization after Giemsa-Eosin staining (red arrows indicated the osteocytes in lacunas). (d) The SEM images of the decellularized bone matrix, and Mg-treated decellularized bone matrix after deposition for 1 h (Mg-enriched (1hr)) and deposition for 4 h (Mg-enriched (4hr)), the typical D-periodicity structure is enlarged in the left-bottom corner. (e) The mechanical properties of the bone matrix treated by decellularization, gamma irradiation (GI) and magnesium plasma surface enhancement were quantitatively verified by nanoindentation (*n = 3*). Error bars indicated means ± standard deviations. Statistically significance is indicated by *$*p < 0.05$, $**p < 0.01$. (For interpretation of the references to color in this figure legend, the reader is referred to the Web version of this article.)

enrichment and density at the superficial solid-liquid interface after magnesium-plasma treatment. Samples were prepared based on decellularized cortical bone slices using the previously described parameters. A commercial SIET system (BIO-001A, Younger USA Sci. and Tech. Corp., USA) was applied and the probe was located 50 μm above the surface on a 30×30 grid after immersing the sample in the aqueous solution (8.059702 mM $Na_2HPO_4 \blacksquare 7H_2O$, 1.4705882 mM KH_2PO_4, 137.93193 mM NaCl, 2.6666667 mM KCl and 1 mM $MgCl_2 \blacksquare 7H_2O$) for 1 h. The obtained data were then analyzed by converting to specific ion outflow (ρmol/cm•s).

The spatiotemporal magnesium environment was characterized by directly analyzing the linear EDS scanning, the initial release, and long-term Mg^{2+} releasing profiles of the magnesium-treated decellularized cancellous bone slices as compared with the control. The parameters for the linear EDS scanning was the similar to the previous test, whereas the transversal surface was utilized. As for the releasing profiles, samples were immersed in 10 ml of simulated body fluid (SBF, pH 7.25) in centrifuge tubes and incubated at 37 °C to monitor the releasing of magnesium cations. The initial release was investigated by measuring the SBF after immersion for 24 h. Thereafter, the SBF was refreshed and collected every 3 days and last for 30 days. At each predetermined time point, the SBF was collected and refreshed while each collected solution was analyzed separately by inductively coupled plasma optical emission spectroscopy (ICP-OES) to determine the magnesium concentration.

2.4. In vitro evaluations of magnesium-treated decellularized bone graft

2.4.1. Cytocompatibility tests

It is believed that the Mg^{2+} concentration and local pH value in the interfacial tissue microenvironment differs from the bulk medium [28], hence, the cytotoxicity of the magnesium cationic cue enriched interfacial TME to hTMSCs was firstly determined by applying the MTT assay. The cell was developed by Professor D. Campana (St Jude Children's Research Hospital, Memphis, Tennessee) [29] and obtained as a gift from Professor Godfrey CF Chan (Department of Paediatrics and Adolescent Medicine, the University of Hong Kong) [30]. The samples that had previously been gamma-irradiated were placed in triplicate wells in 24-well plates, and 100 μL of cell suspensions containing $6*10^5$ cells/ml were seeded in each well. Cells were cultured for 4 h before a 900 μL culture medium was added. The cells were cultured using the Dulbecco's Modified Eagle Medium (DMEM, Invitrogen, USA) supplemented with 10% fetal bovine serum (FBS, Biowest, France), antibiotics (100 U/ml of penicillin and 100 μg/ml of streptomycin) and 2 mM L-glutamine at 37 °C in an incubator under 5% CO_2 and 95% air for 1 or 3 days. At each time point, the MTT solution, which was prepared by dissolving thiazolyl blue tetrazolium bromide powder in phosphate buffered saline (PBS, OXOID Ltd., England), was added and cultured in the incubator for 4 h. Afterwards, 100 μL of 10% sodium dodecyl sulphate (SDS, Sigma, USA) in 0.01 M hydrochloric acid was added to each well and incubated overnight. Consequently, the optical density was recorded at 570 nm with a reference of 640 nm using the plate reader (MULTISKAN GO, Thermo Scientific, USA). Cell viability was determined from the absorbance values.

The same cell-culturing process was applied to observe the cell morphology of hTMSCs when cultured with different samples on days 1 and 3. At appropriate time points, the cells were fixed with a 10% neutral buffered formalin solution and then dehydrated in an up-grading series of the ethanol solution at room temperature. Finally, the samples were dried in a critical point dryer using liquid carbon dioxide as a transitional fluid before coating with a thin gold layer. The cell morphology was then observed with SEM.

2.4.2. Cell proliferation

Following a previously reported protocol [31], a BrdU Incorporation ELISA Kit (Roche, USA) was used to study cell proliferation while culturing with the samples. Briefly, the hTMSCs, at a density of $3*10^5$ cells/cm^2 were cultured with the gamma-irradiated samples for 4 h before topped up culture medium to 1 mL. At each predetermined time interval, which is 1 day and 3 days of cultivation, respectively, the BrdU solution was added to label the cells for 4 h. Consequently, the labelled cells were fixed at room temperature for 30 min before incubating with an *anti*-BrdU-POD solution for 2 h. Afterwards, they were rinsed several times with PBS, and the substrate solution was then added. Finally, the reaction was stopped by adding 1 M H_2SO_4, and the absorbance was recorded using a plate reader at 450 nm. The proliferation rate at each time interval was normalized to the absorbance obtained from the corresponding control group individually.

2.4.3. Osteogenic differentiation

The osteogenic differentiation property of the magnesium cationic cue enriched interfacial tissue microenvironment compared to that of the control was investigated by assaying the alkaline phosphatase (ALP) activity on day 3, day7 and day 14, when cultured with hTMSCs, respectively. Similar to the previous assay, $5*10^5$ cells/cm^2 cells were first incubated with the bone slices in a 24-well plate for 1 day. The medium in each well was then replaced with osteoinductive medium (OI medium) containing 50 μg/ml ascorbic acid (Sigma, USA), 10 mM of β-glycerol phosphate (MP Biomedicals, France), and 100 nM dexamethasone (Santa Cruz, UK) and changed every 3 days afterwards. At each time point, the cells were washed several times with PBS and then lysed with 1% Triton X-100 at 4 °C for 1 h. The lysates were centrifuged at 4 °C for 10 min under 574 g, and the ALP activity of each sample was determined by assaying the supernatant using a *p*-nitrophenyl phosphate (*p*-NPP) reagent (Stanbio, USA). The absorbance was recorded by the plate reader at a wavelength of 405 nm. The total protein level obtained from the Bio-Rad Protein Assay (Bio-Rad, USA) was applied to normalize the ALP activity.

2.4.4. Cell mineralization

The cell mineralization was evaluated using alizarin red S staining by culturing hTMSCs with the samples. Similar to the previous cell-seeding process, an aliquot of 1 ml cell suspensions containing $1*10^5$ cells/ml cells was cultured with the magnesium-treated decellularized bone slices or with the decellularized control, and the culturing conditions and processes were the same as those used in the ALP assay. After incubating for 28 days, the samples were washed several times with PBS (pH ~4.1) and fixed with 10% paraformaldehyde for 30 min. Afterwards, they were rinsed again with PBS (pH ~4.1) prior to the addition of 1% alizarin red S staining solution (pH ~4.1). The samples were incubated in the dark and at room temperature for 20 min and visualized by optical microscopy. Image J software was then applied to analyze the photos. The final result was exhibited in the form of a mineralized area to the corresponding total area of the surface. Quantification analysis was performed by dissolving the staining using 10% cetylpyridinium chloride, and the absorbance at 562 nm was recorded.

2.4.5. Quantitative reverse transcription polymerase chain reaction (qRT-PCR)

The osteogenic responses of hTMSCs in terms of relative mRNA expression levels of several typical osteogenic markers, including alkaline phosphatase (ALP), runt-related transcription factor 2 (Runx2), Type I collagen (Colla1) and osteocalcin (OCN), were subsequently analyzed by real-time qRT-PCR. The primer pairs used are shown in Table S1. The cell incubation conditions and processes were the same as those used in the ALP assay. Cells were cultured for 3, 7, 14 and 21 days, respectively, and the total RNA was then extracted using Trizol reagent (Takara, Japan) following the manufacturer's instructions. Afterwards, cDNA was synthesized with PrimeScript RT reagent kit (Takara, Japan). Subsequently, the real-time PCR was performed using the SYBR Green PCR Master Mix (Applied Biosystems, USA). A 25 μL solution containing 12.5 μL 2 × SYBR Green PCR Master Mix, 1 μL of forward and 1 μL of reverse primers, 1 μL of cDNA template and 9.5 μL of RNase water was

applied, and the reaction was carried out on the ABI Prism 7900HT sequence detection system (Applied Biosystems, USA) for 40 cycles with standard setting. Finally, the relative mRNA expression level of each gene was normalized to the house-keeping gene glyceraldehyde-3-phosphate dehydrogenase (*Gapdh*) and determined using Ct values. All the experiments were performed in quintuple.

2.5. Osseointegration assessments of magnesium-treated allograft bone in rat defect model

2.5.1. Graft preparation and surgery

The preparation of decellularized allograft bone from carcasses of SD rats is delineated in the previous paragraph. After that, a tiny hole was drilled at the edge of the end of the bone rod to allow the sample to be hung within the chamber (Fig. S1). The customized plasma treatment parameters were applied. Finally, all samples were gamma-irradiated at a dose of 30 KGy and stored before surgical implantation.

The SD rats were used to perform the *in vivo* assessments in terms of osseointegration and osteogenic response of the magnesium-treated allograft bone. The anaesthetic, surgical and post-operative care protocols were examined by and fulfilled the requirements of the University Ethics Committee of the University of Hong Kong and the Licensing Office of the Department of Health of the Hong Kong Government.

Eighteen SD rats with 14 weeks old and weighing about 250–350 g obtained from the Laboratory Animal Unit of the University of Hong Kong, were used and six rats were involved in each group. The right lateral epicondyle was chosen as the operation site. A perforative hole with a depth of approximately 6 mm and a diameter of 2.2 mm was drilled across the right lateral epicondyle of each rat, and either a magnesium-treated or control allograft bone was implanted before sutured. Three rats in each group were euthanized on day 10 and the others were sacrificed on day 28.

2.5.2. Micro-computed tomography evaluation

Micro-computed tomography was applied to monitor the changes of bone volume and bone mineral density of bony tissue and responses of surrounding tissue within the operation site at different time points, including day 0, 3, 10, 21 and 28. The live rats were directly scanned in the micro-CT machine (SKYSCAN 1076, Bruker, Germany), and the 2D planes were subsequently reconstructed using the NRecon (Skyscan Company), while the 3D models were reconstructed by CTVol software (Skyscan Company).

2.5.3. Histological evaluation

The rats were euthanized on day 10 and day 28 post-operation and all the femora implanted with allograft bone were retrieved. Samples from two rats in each group were fixed in 10% neutral buffered formalin (NBF) for 72 h, followed by decalcification in 10% EDTA (pH 7.4) and standard processing for paraffin embedding. Serial paraffin sections were cut at the 7 μm thickness, and fast green-safranin O (F&S) staining was then performed with paraffin-embedded slices. Optical microscopy was applied for the morphological and histological observation and analysis.

2.5.4. Elemental mapping on the in vivo specimens

The elemental mapping was performed on PMMA-embedding sections. One specimen from each group were collected at 10 days and 28 days post-implantation, respectively, and extra tissue and compound were removed before fixed in 10% NBF for 3 days. Dehydration of specimens with grades of ethanol was performed, followed by bathing in xylene for 3 days. Subsequently, all samples were embedded in methyl methacrylate (MERCK, Germany) for further polymerization. The PMMA-embedded samples were sectioned and finally micro-ground to 50–70 μm sections, and the analysis was performed via EDS through direct testing of the PMMA-embedded sections.

2.5.5. Nanoindentation of the regenerative bone tissue

A nano-indenter (Nano Indenter G200, USA) was employed to test Young's modulus of the newly formed bone at 28 days post-implantation following a method reported in the literature [32]. Briefly, a Berkovich tip with a radius of 20 nm was applied as an indenter to directly punch the PMMA-embedded sections using fused silica and single-crystal tungsten as reference materials. The constant value of the Poisson ratio, maximum indentation depth, maximum load, peak holding-time, and drift rate were set at 0.35, 4000 nm, 10 mN, 120 s, and 1.2 nm/s, respectively. The Oliver-Pharr method was applied to calculate Young's modulus. This protocol applies to other nanoindentation test mentioned in this study.

2.6. Evaluation of integrin-mediated cell adhesion

Several integrin subunits expressed by MSCs (e.g. ITGA3, ITGA5, ITGB1 & ITGB3) were targeted, and the primer pairs used were shown in Table S1. The cell incubation conditions and processes were the same as those used in the MTT assay. Cells were cultured for 24 h and the experimental protocol was exactly the same as previously described. All the experiments were performed in quintuple.

The mouse monoclonal antibodies against human integrin α_3 and α_5 were purchased from Abcam (ab20141, ab78614). For the cell adhesion test after antibody-blocking, hTMSCs were first pre-incubated in suspension with corresponding integrin antibodies with a final concentration of 10 μg/mL for 15min at 37 °C. These pre-treated cells and untreated hTMSCs were then incubated with the decellularized control, the Mg-enriched (1hr) and the Mg-enriched (4hr) samples, and the corresponding antibodies were added to the culture medium (10 μg/mL) for each group. After incubation for 24 h, the slices were gently washed with PBS to remove loosely adherent cells. The adhesion cells in each group were subsequently analyzed by MTT assay.

In order to further verify the integrin-mediated cell adhesion in the Mg cationic cue enriched interfacial TME, hTMSCs were transfected with commercially available siRNA targeting integrin α_3 and α_5 (Santa Cruz, UK) following the manufacturer's instructions. One day before transfection, subconfluent hTMSCs were cultured in antibody-free DMEM, supplemented with 10% FBS. Cells were incubated with a complex formed by the siRNA, the transfection reagent (Santa Cruz, UK), and the transfection medium (Santa Cruz, UK) for 7 h at 37 °C. A control siRNA sequence (Santa Cruz, UK) was used as a negative control. Afterwards, the medium was changed into normal medium containing 10% fetal bovine serum and antibiotics, and the hTMSCs were cultured for another 24 h.

Immunoblots for integrin α_3 and α_5 were used to test the efficiency of RNA-silencing in the hTMSCs. Afterwards, these pre-treated cells and untreated hTMSCs were incubated with Mg-enriched (1hr) and Mg-enriched (4hr) samples, respectively, for 24 h, and MTT assay was applied to test the adhesion cells in each group after the loosely adherent cells were gently removed by PBS washing.

2.7. Statistical analysis

The *in vitro* experiments were performed in triplicate or quintuple, and the *in vitro,* as well as the *in vivo,* experimental data were analyzed using the one-way ANOVA method, the final results were expressed as mean $\pm$ standard deviations (SD). A *p* value < 0.05 was considered to be statistically significant.

3. Results

3.1. Morphology characterizations of bone slices after decellularization

The morphology of decellularized bone slices was observed under a light microscope after Giemsa-Eosin staining and scanning electron microscopy, respectively (Fig. 1c and d). As demonstrated, the medulla

material was found completely removed, while the microporous structure was maintained. In addition, the collagen fibrils, especially the *D*-periodicity, could still be clearly identified. According to the Giemsa-Eosin staining, the blue dots highlighted by red arrows represent osteocytes present in the lacunas of the bone matrix, whereas these dots could not be found in the processed bone matrix. This evidence confirms the success elimination of the residual soft tissue, while the structural integrity of the bone matrix was maintained in both groups.

3.2. Characterizations of magnesium-treated decellularized bone graft

3.2.1. Surface morphology

The surface morphology of processed bone graft, especially the collagen-like structure after the magnesium treatment was examined under SEM and is displayed in Fig. 1d. By employing a set of magnesium treatment, the surface morphology was well-maintained. The collagen-like structures could be identified easily, and their fibrils likely exposed.
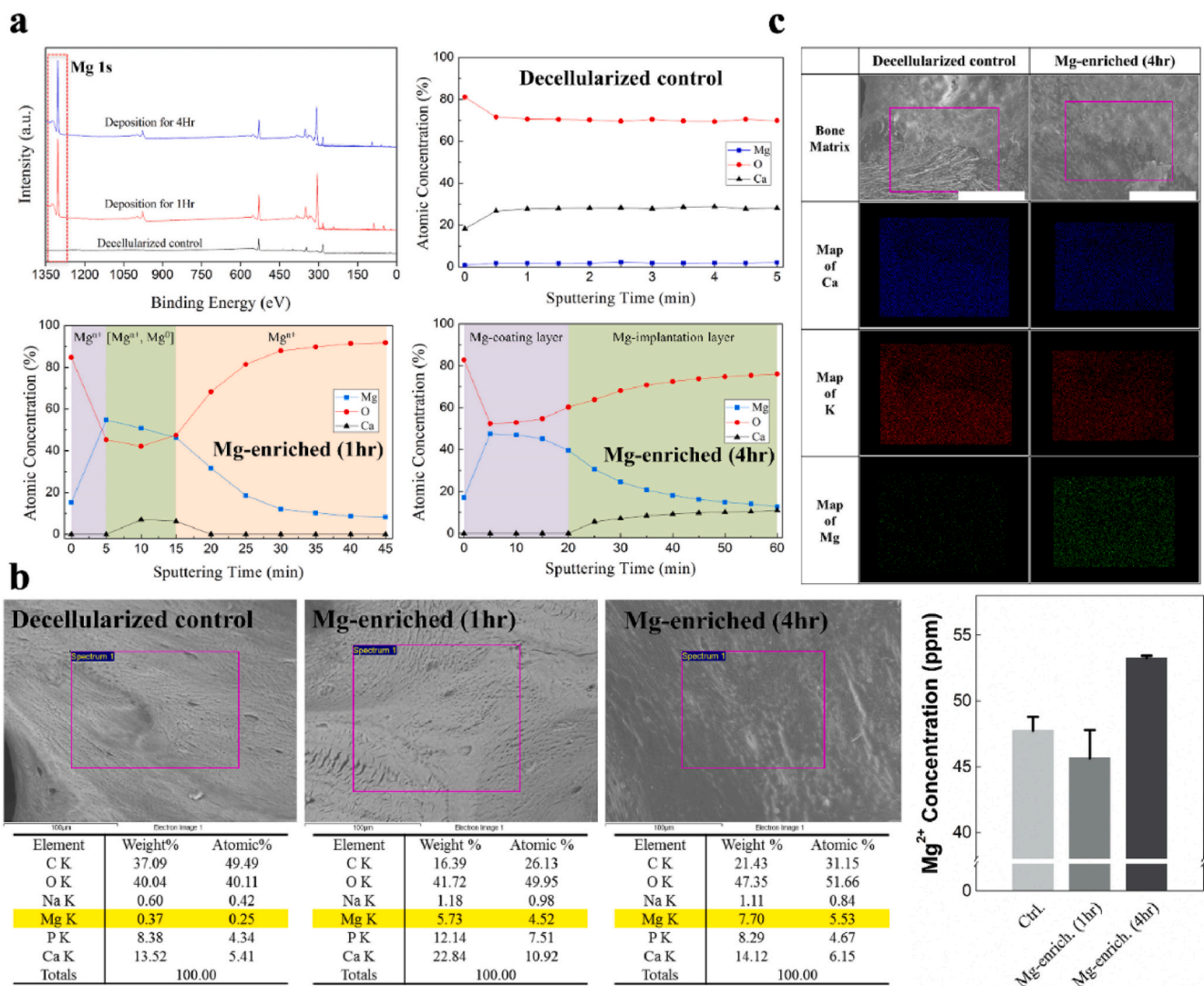
3.2.2. Mechanical properties

Young's modulus and the hardness of different bone matrix have been characterized by nanoindentation tests, and the results are depicted in Fig. 1e. No structural difference was observed between both groups though. The Young's modulus of the treated bone matrix and control were generally reduced after gamma irradiation (GI). However, no significant difference was found between the Mg-treated samples and the control in terms of mechanical properties. This indicates that the magnesium treatments would not jeopardize the structural integrity of the bone matrix.

3.2.3. Surface elemental composition and magnesium depth profile

XPS result confirms the existence and chemical state of magnesium in the near surface of the Mg-treated decellularized samples compared to the control (Fig. 2a). A strong signal at 1305e from the Mg-treated samples was attributed to Mg 1S (Mg^{n+}) and was not evident in the decellularized control. The elemental depth profiles of untreated and Mg-treated cortical bone grafts were further obtained via an XPS sputtering technique; the results are shown in Fig. 2a. Relatively low magnesium concentrations were detected from the untreated samples, while the concentrations of calcium and oxygen were nearly 30% and 70%, respectively. Specific to the sample that been deposited for 4 h, different regions were delineated according to the proportions of magnesium and oxygen, where the specifically tailored surface structure composed of

Element	Weight%	Atomic%
C K	37.09	49.49
O K	40.04	40.11
Na K	0.60	0.42
Mg K	0.37	0.25
P K	8.38	4.34
Ca K	13.52	5.41
Totals		100.00

Element	Weight %	Atomic %
C K	16.39	26.13
O K	41.72	49.95
Na K	1.18	0.98
Mg K	5.73	4.52
P K	12.14	7.51
Ca K	22.84	10.92
Totals		100.00

Element	Weight %	Atomic %
C K	21.43	31.15
O K	47.35	51.66
Na K	1.11	0.84
Mg K	7.70	5.53
P K	8.29	4.67
Ca K	14.12	6.15
Totals		100.00

Fig. 2. Surface characterizations of the control and magnesium-enriched bone grafts. (a) XPS examination of decellularized control and Mg-treated bone grafts; the highlighted square exhibits the signal of Mg element. Depth profile of Mg element on the surface of decellularized control, Mg-enriched (1hr) graft, and Mg-enriched (4hr) graft. (b) Surface chemical compositions of different bone grafts obtained from EDS tests and the relative weight percentages of the magnesium are highlighted. (c) Element mapping acquired from the decellularized control and Mg-enriched graft (Scale bar = 200 μm).

Mg-coated layer and transitional layer could be clearly distinguished. In the 680 nm depth on the top, no calcium was detected; after that, the calcium was recognized, which was attributed to the bone matrix. This confirmed that magnesium compounds predominated in the top surface layer, with a thickness about 680 nm. The layer underneath was composed of mixture of pure magnesium and magnesium compounds, while the transitional layer was predominated by magnesium compounds. On the other hand, the specifically tailored surface profile was not exerted on the control sample.

Apart from the XPS, EDS was also utilized to detect the Mg content on the Mg-treated samples and the control (Fig. 2b and c). The relative weight percentage of magnesium in the surface layer of decelluarized bone graft was only 0.37%. After being deposited with magnesium for 1 h and 4 h, the value increased dramatically to 5.73% and 7.70%, respectively. Subsequently, the elemental distribution in the surface layer of selected samples was analyzed by EDS elemental mapping (Fig. 2c). As the basic elements in bone, large amounts of calcium (Ca) and phosphate (P) from untreated and Mg-treated bone graft were detected. However, the magnesium on the surfaces of the untreated sample was quite low compared with that of the Mg-treated sample. Meanwhile, the magnesium in the Mg-treated sample was evenly distributed.

3.2.4. Analysis of interfacial and spatiotemporal magnesium microenvironment

The results of the interfacial Mg microenvironment was detected and confirmed by the mean of SIET method, and the Mg^{2+} flow rate over the surface of the Mg-treated bone slices are depicted in Fig. 3a. After treated by customized protocol, the interfacial Mg^{2+} flow rate of the Mg-enriched (4hr) graft reached 5000 $\rho Mol\ cm^{-2}\ s^{-1}$ approximately, whereas the value of the Mg-enriched (1hr) sample was slighted increased to 1000 $\rho Mol\ cm^{-2}\ s^{-1}$. It is thus firstly been confirmed that the magnesium cationic cue enriched interfacial microenvrinomet can be tailored over the surface of allograft bone by appliying the customized magnesium treatment method.

Regarding the spatiotemporal magnesium envrionment, several tests were confucted. In the 24-hr immersion testing, the magnesium concentration of Mg-enriched (4hr) graft was slightly higher than that of the decellularized control but not the Mg-enriched (1hr) graft (Fig. 3b). The long-term releasing of the magnesium in the medium was tested by ICP-OES (shows in Fig. 3c), and the magnesium content obtained from the Mg-enriched (4hr) and Mg-enriched (1hr) samples were slightly higher than those of the decellularized control, respectively, with values maintained in the range of 50–60 ppm. The curves obtained from linear EDS scanning showed that the Mg distribution in the transversial surface of plasma-treated samples was similar to that of the untreated control (Fig. 3d), implying the magnesium contents within the allograft bone was not altered after magensium treatments.

There results implicated that magnesium ion enriched interfacial tissue microenvironment was successfully established over the bone surface whereas the spatiotemoporal magnesium environment was only slightly been affected, with the utilizaion of the specifically designed magnesium-plasma treatments, and this can hardly be achieved in synthetic bone substitutes.
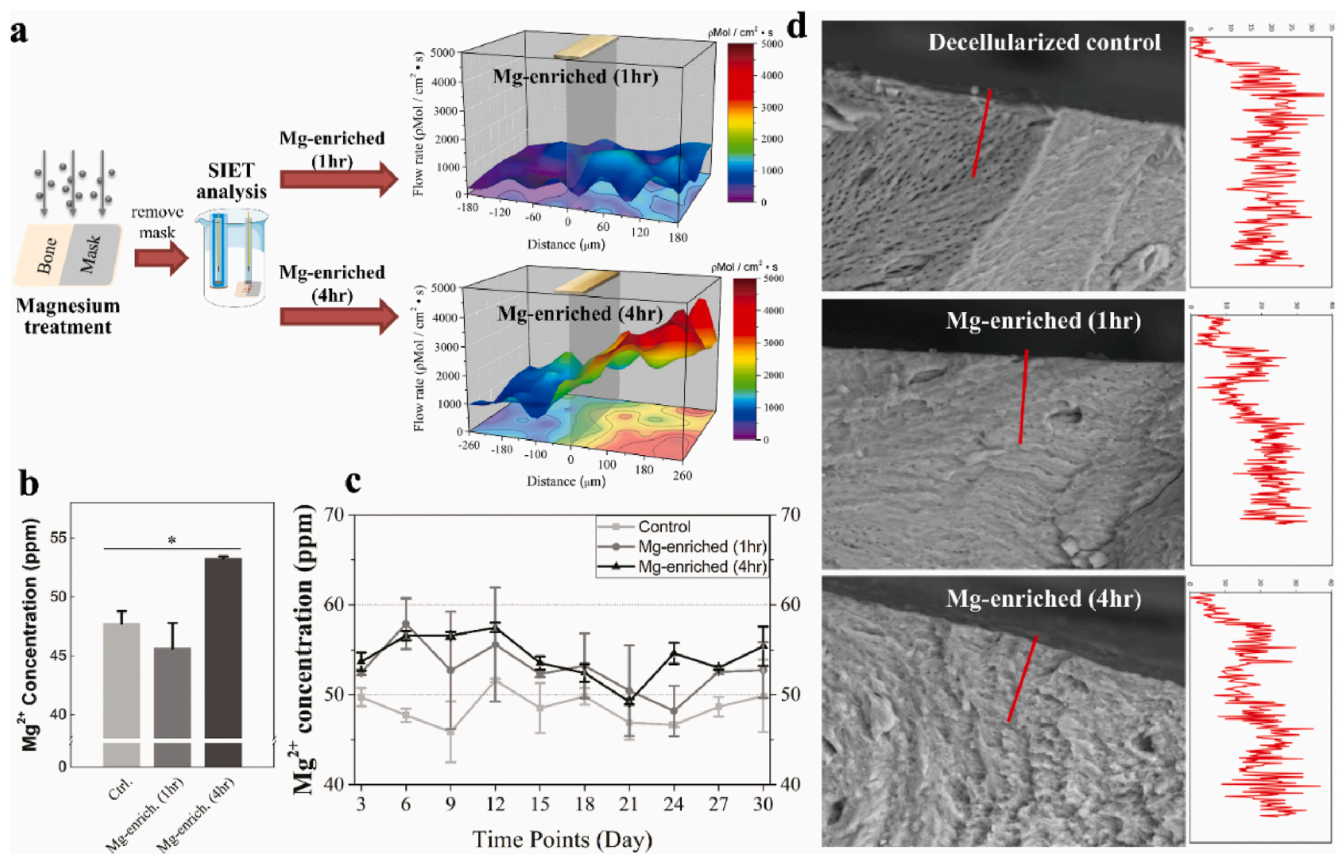
Fig. 3. Characterizations of magnesium cationic cue in the bone tissue microenvironment. (a) Scheme of the SIET analysis and the interfacial Mg microenvironment in terms of the Mg^{2+} flow rate over the surface of Mg-treated bone slices, for which half of the surface was covered while the other half was not. The plane at "0" represents the outline of these two different areas, and the image of the sample has been included at the top of each 3D-colormap surface. The spatiotemporal Mg environment after Mg-plasma treatment were also comprehensively characterized. (b) The initial release of different samples after immersion in SBF for 24 h and (c) long-term Mg concentration of control and different Mg-treated samples, $n = 3$. Error bars indicated means ± standard deviations. Statistical significance is indicated by $*p < 0.05$ as compared with gamma-irradiated control. (d) The Mg distribution in the transversal surface of the control and magnesium-treated grafts.

3.3. In vitro evaluations of magnesium-treated bone graft

3.3.1. Cytocompatibility tests

Fig. 4a shows the visualized cell morphology of hTMSCs after cultured on different samples for 24 h via SEM. Cells were attached to the surfaces of both decellularized and Mg-treated bone slices. Meanwhile, they were well spreading on Mg-treated samples, and higher coverage was depicted on the Mg-enriched (4hr) graft as indicated by the reduced area of the yellow color.

The cytocompatibility of the Mg-enriched grafts compared to the control sample were assayed via MTT method. The cell viability of hTMSCs after 1 and 3 days of culturing are depicted in Fig. 4b. On day 1, the viability of hTMSCs incubated with Mg-enriched bone graft was in the range of 120–140%, showed significant increasing of cell viability. This trend was similar when cultured for 3 days, but the increasing was not significant.

3.3.2. Cell proliferation

The cell proliferation of hTMSCs, which was indicated by the fold change of BrdU incorporation, is exhibited in Fig. 4c. After 24-hr incubation, cells cultured with the Mg-enriched (4hr) bone graft exhibited significantly higher BrdU incorporation, reaching to about 140%, compared to those of the control and Mg-enriched (1hr) samples. After reaching the highest proliferation rate, the value for the Mg-enriched (4hr) graft dropped to about 90% on day 3, which may be attributed to the limited surface area for cell proliferation and the trends towards osteogenic differentiation.

3.3.3. Alkaline phosphatase (ALP) activity

The osteogenic response of hTMSCs cultured with untreated and Mg-treated decellularized bone graft were revealed in the form of ALP activities after 3, 7 and 14 days of incubation, as demonstrated in Fig. 5a. Significantly higher ALP activity was observed in cells cultured with Mg-enriched (4hr) graft and peaked on day 7 with value of about 180 U mg^{-1} protein, while the activity of the decellularized control and Mg-enriched (1hr) graft were at about 120 U mg^{-1} protein at the same time point. After 14 days of culturing, similar ALP activities were found in cells cultured with Mg-enriched (4hr) graft compared to the other samples.

3.3.4. Mineralization and calcium deposition

The mineralization of cells was assayed by culturing with different cancellous bone grafts. As exhibited in Fig. 5b, the porous structure of the cancellous bone grafts was gradually occupied by the secreted and deposited calcium content; the difference can be identified via Image J analysis. For the control samples, approximate 15% was occupied, while the numbers were estimated at 19% and 34% for the Mg-enriched (1hr) and Mg-enriched (4hr) graft, respectively.

3.3.5. mRNA expression of osteogenic markers

Afterwards, mRNA expression level of the four typical osteogenetic markers expressed by hTMSCs, including ALP, Runx2, Collα1 and OCN, were analyzed at different time points (Fig. 5c). The gene expression levels of ALP and Collα1 in the cells cultured with Mg-enriched (4hr) graft were significantly promoted and peaked at Day 3, with the values to be about 6-fold and 10.7-fold higher, respectively. Regarding the Runx2 and OCN from the same batch of cells, the expression level of those cultured with Mg-enriched (4hr) bone graft showed maximum value at Day 7, and the value was elevated about 8.6-fold and 2.8-fold, respectively. Meanwhile, the mRNA expression level from the Mg-enriched (1hr) graft were similar to that from the decellularized control.
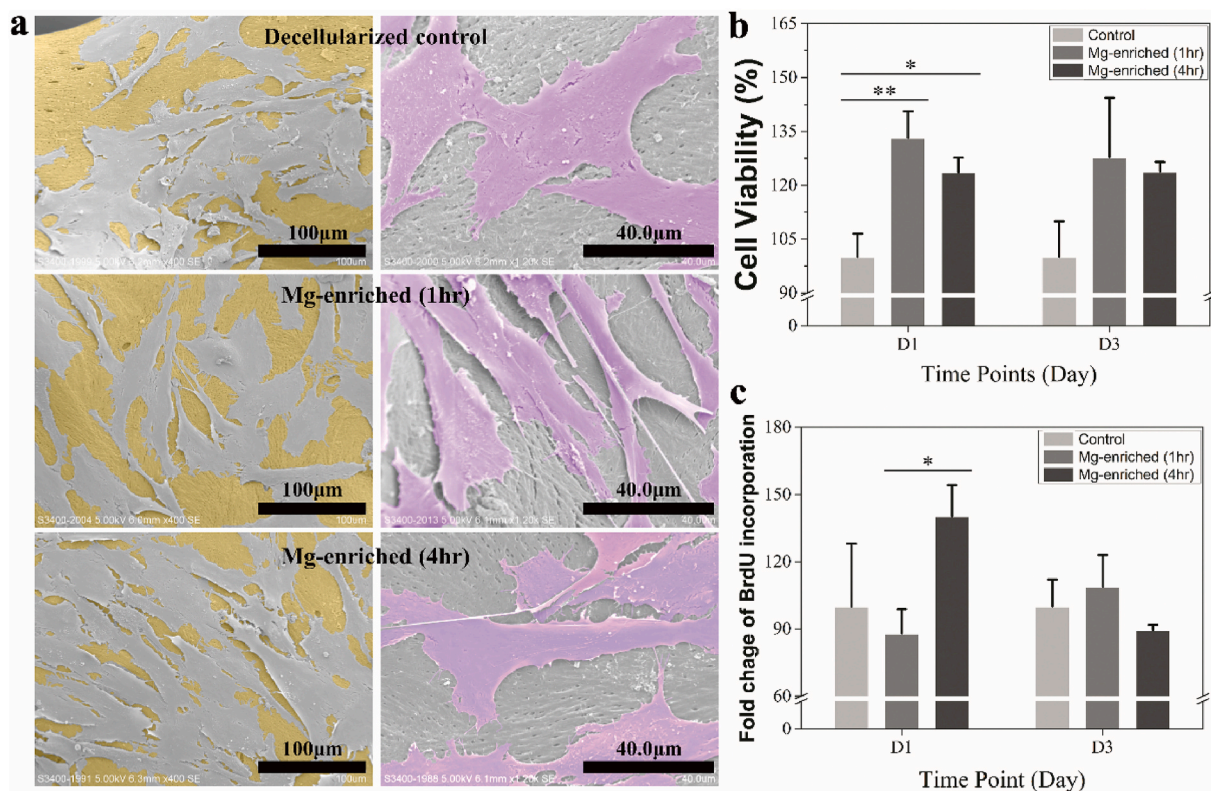
Fig. 4. *In vitro* cellular morphology and proliferation of hTMSCs in the Mg^{2+}-enriched interfacial tissue microenvironment. (a) Cell density and morphology of hTMSCs when cultured with decellularized control, Mg-enriched (1hr) graft, and Mg-enriched (4hr) graft under SEM. (b) Cell viability of hTMSCs cultured with different samples determined by MTT assay (*n* = 3). (c) Cell proliferation of hTMSCs after incubated with different samples determined by BrdU-labeling assay (*n* = 3). Error bars indicated means ± standard deviations. Statistically significance is indicated by *$p < 0.05$, **$p < 0.01$.
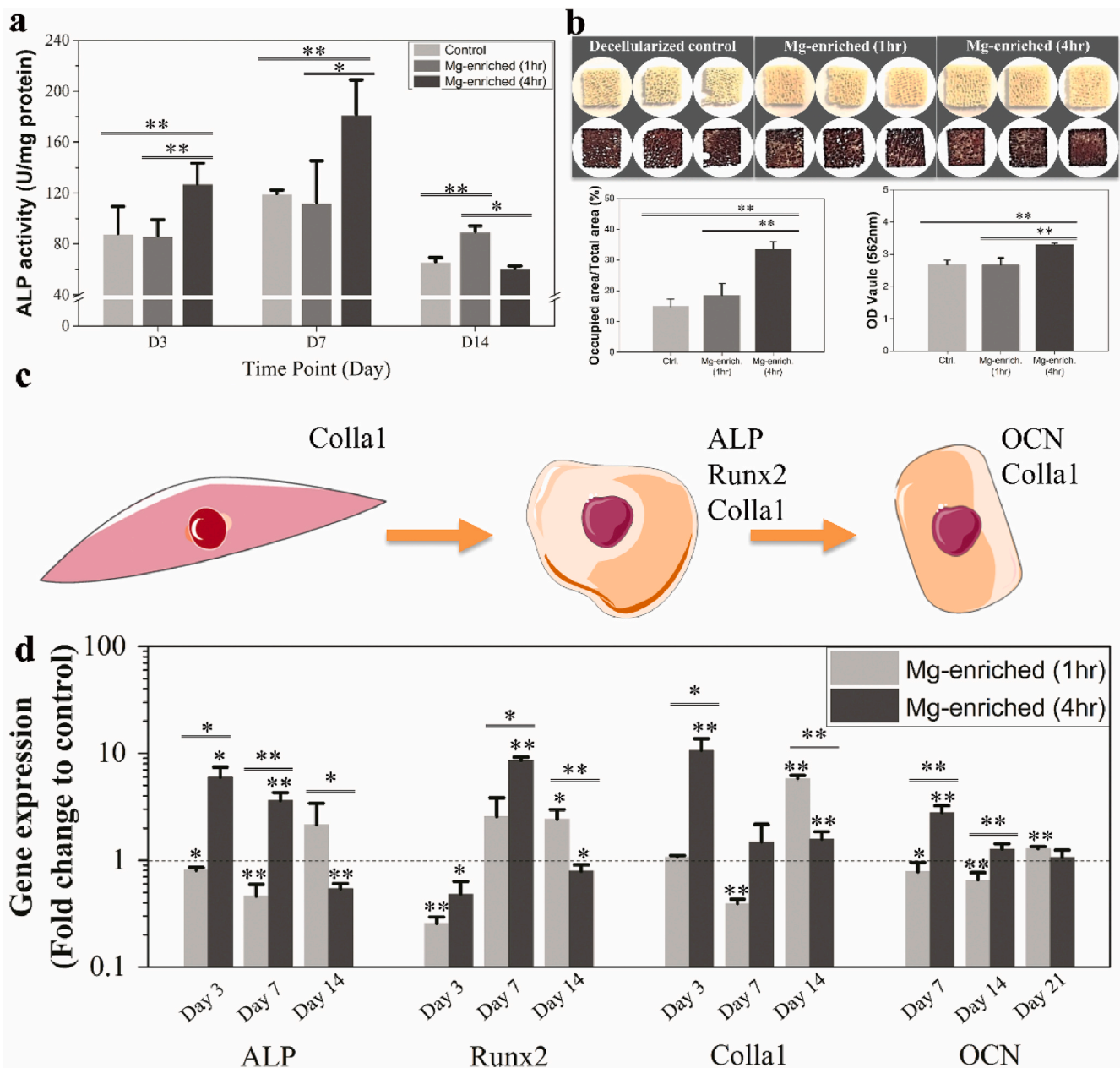
Fig. 5. *In vitro* osteogenic responses of hTMSCs in the Mg^{2+}-enriched interfacial tissue microenvironment. (a) Osteogenic effects of decellularized control and Mg-treated bone slices when cultured with hTMSCs determined by measuring ALP activities at different time points ($n = 3$). (b) Mineralization of hTMSCs incubated with different samples for 28 days determined via alizarin red S staining. The porous structure was gradually occupied. The semi-quantitative result and quantification analysis were exhibited accordingly ($n = 3$). (c) Typical markers been monitored for MSCs, pre-osteoblasts and osteoblasts during osteogenic differentiation and (d) the relative mRNA expression level of these markers, including alkaline phosphatase (ALP), runt-related transcription factor-2 (Runx2), collagen type I alpha I (Colla1) and osteocalcin (OCN), detected from hTMSCs cultured with different samples at specific time points determined by RT-qPCR tests ($n = 5$). Error bars indicated means ± standard deviations. Statistically significance is indicated by *$p < 0.05$, **$p < 0.01$. (For interpretation of the references to color in this figure legend, the reader is referred to the Web version of this article.)

3.4. Osseointegration assessments of magnesium-treated allograft bone in rat bone defect model

3.4.1. Micro-computed tomography evaluation

The images of the cross section of the right femur implanted with either untreated allograft bone or magnesium-treated samples (mg-enriched (1hr) and mg-enriched (4hr) graft) at particular time points obtained from micro-CT are displayed in Fig. 6a; the defect sites are highlighted. During the first 3 days, the morphology of the implants and the defects was not changed. On day 7 and day 10, the differences between the untreated grafts and the Mg-treated grafts began to appear,

and bone tissue around the control grafts lost; however, bony ongrowth was observed at the periphery of Mg-enriched (4hr) grafts. Subsequently, the defect site implanted with Mg-enriched (4hr) allograft bone was gradually filled by regenerated bone tissue, whereas voids can still be recognized in the site implanted with Mg-enriched (1hr) or control allografts.

Accordingly, 3D reconstructions were made based on the volume of interest (VOI), which is a cylinder with a cylinder with a diameter of 2.74 mm and 4 mm high. During the first 10 days, the bone resorption activity predominated, and the distinct reduction of bone volume was revealed in both groups. After 10 days, obvious ongrowth of new bone
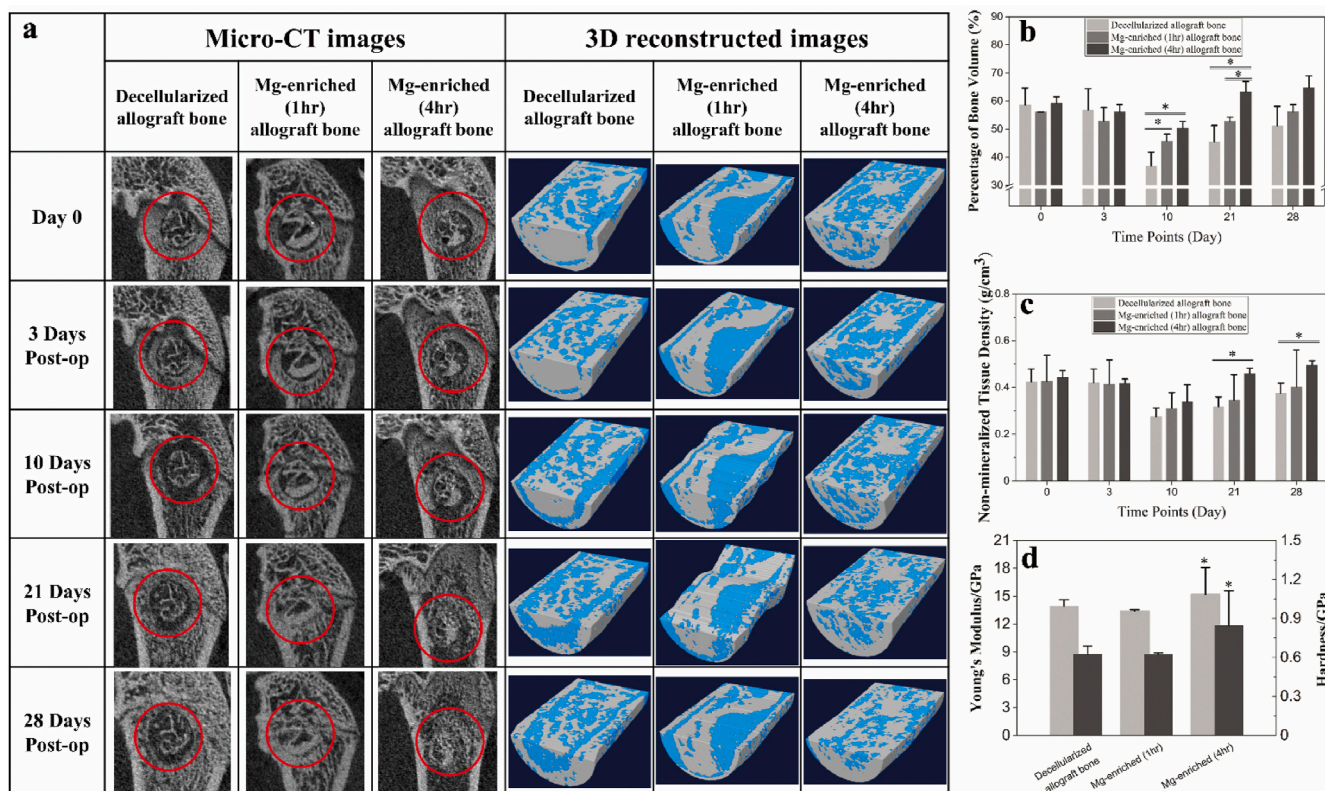
Fig. 6. *In vivo* evaluation of new bone formation by micro-computed tomography and nanoindentaiton. (a) Representative Micro-CT scanning images and 3D reconstructed images. The percentage change of (b) bone volume, (c) non-mineralized tissue density, and (d) mechanical properties was also quantitatively calculated using the Micro-CT scanning and the nanoindenter, respectively, $n = 3$. A total of eighteen rats were used, i.e., $n = 6$ in each group. Error bars indicated means ± standard deviations. Statistically significance is indicated by $*p < 0.05$.

appeared in the area surrounding the Mg-enriched (4hr) allograft bone; ingrowth was also observed on day 28. However, the new bone formation was found on day 21 for the control groups and there were no clear changes in bone volume at the central part of the graft. This difference is indicated by the quantitative analysis calculated from the micro-CT data (see Fig. 6b), in which significantly increased bone volume was found on post-operative day 10 and day 21.

As illustrated in Fig. 6c, the restoration of the non-mineralized tissue density was showed at 21 days post-operation when the Mg-enriched (4hr) allograft bone had been implanted, indicating that the regenerated non-mineralized tissue might have subsequently mineralized into bone tissue, whereas the values for the control groups were not yet restored. In order to test this hypothesis, nanoindentation tests were performed 28 days after implantation to measure Young's modulus and the hardness of the bone tissue, and the results are presented in Fig. 6d. The modulus of the bony tissue from the defects implanted with Mg-enriched (4hr) allografts was 15.17 ± 2.92 Gpa, while the modulus of the Mg-enriched (1hr) graft and control samples was 13.90 ± 0.69 GPa and 13.397 ± 0.16 GPa on average, respectively. This indicates that the bone was more mature when the Mg-enriched (4hr) allograft bone was used.

3.4.2. Histological evaluation

The histological images of the defects implanted with the different samples are presented in Fig. 7a. In the bony tissue microenvironment, both of the bone healing processes caused an underlying inflammatory reaction on 10 days post-operation. Abundant fibrous tissue emerged around the implants and filled the gaps between the allograft bone and host bone. Four weeks later, the loose fibrous tissue was gradually replaced by dense, bone-like tissue in the Mg-enriched (4hr) graft group. With the ingrowth of the newly formed bone, the boundary between the

implant allograft and the host bone became undifferentiated. However, the healing process was different for the defects implanted with gamma-irradiated allograft bone, where the bone-like tissue was less dense. In addition, the cartilaginous-like tissue can still be found in the control group at 28 days post-implantation, as indicated by the red arrow.

### 3.4.3. Elemental mapping on the in vivo specimens

The energy-dispersive X-ray spectroscopy (EDS) technique was utilized to map the Mg-enriched (1hr), Mg-enriched (4hr) and control allografts at different time points post-implantation. The bone tissue within the section was distinguished by detecting the presents of calcium (Ca) and phosphate (P), and the elemental maps are shown in Fig. 7b. On post-operative day 10, semi-quantitative calculation showed a higher percentage of magnesium (2.05 wt%) in the defects implanted with Mg-enriched (4hr) allograft bone than that in the decellularized graft (0.86 wt%) and the Mg-enriched (1hr) graft (0.99 wt%). These values were reduced on 28 days after implantation (Figs. S2–4).

3.5. Molecular biological analysis of mesenchymal stem cells adopted to magnesium cationic cue enriched interfacial tissue microenvironment

The gene expression levels of several integrin subunits expressed by hTMSCs were analyzed after culturing with different grafts for 24 h (Fig. 8a). Interestingly, it was found that the expression level of integrin α_3 and α_5 in hTMSCs cultured on the Mg-enriched (4hr) grafts was significantly elevated 5.2-fold and 5.4-fold, respectively, compared to the untreated controls, while the expression levels were reduced for those cultured on the Mg-enriched (1hr) grafts. However, no notable difference in the mRNA levels of integrin β_1 and β_3 was found between the hTMSCs cultured with the Mg-enriched sample and those cultured with the controls.
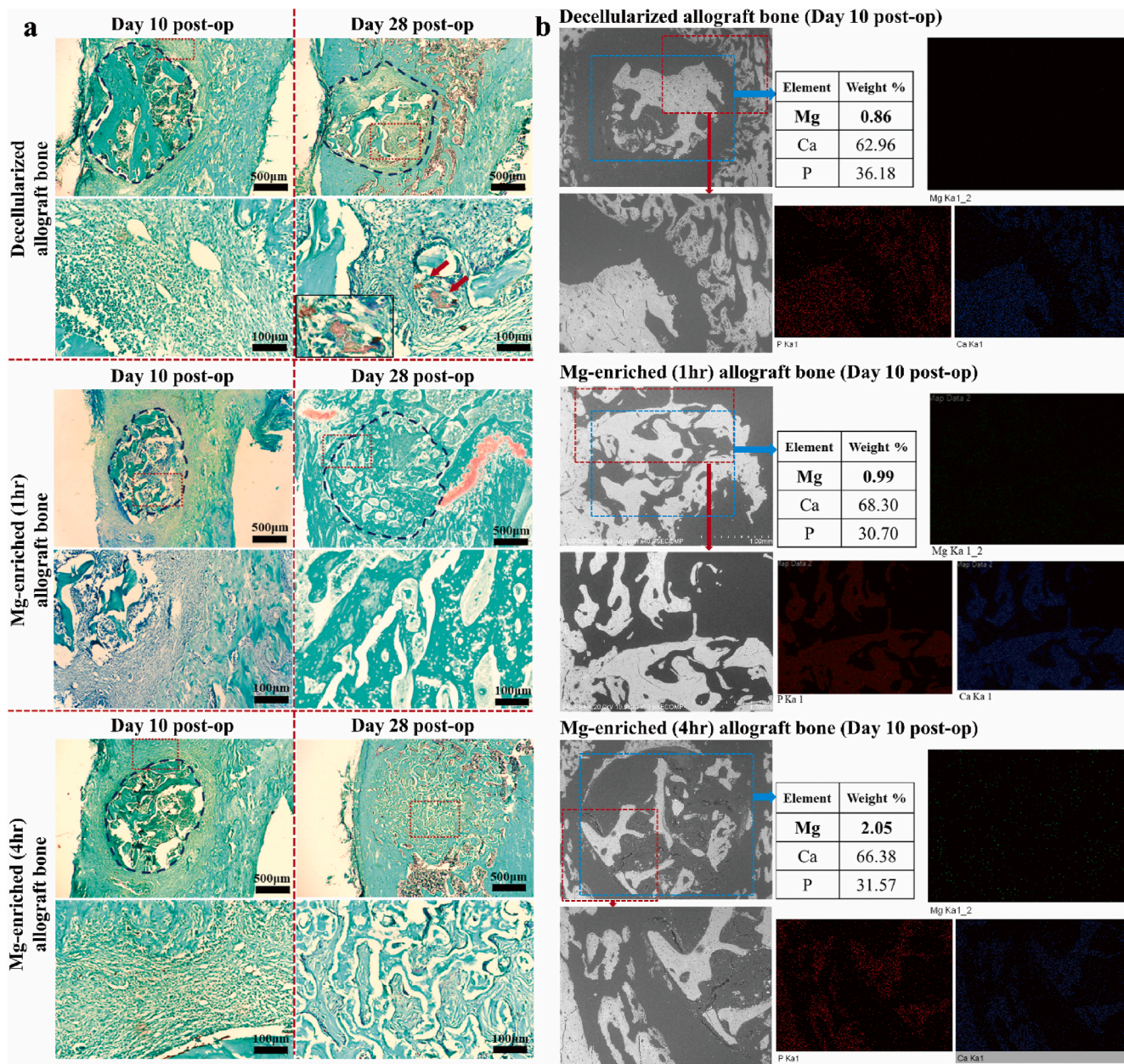
Fig. 7. *In vivo* characterizations of osseointegration and Mg-enriched bone tissue microenvironment of bone allografts in rat animal model. (a) Histological photographs of decellularized, Mg-enriched (1hr) and Mg-enriched (4hr) allografts stained with fast green & safranin O after 10 days and 28 days implantation, respectively. (a) Left Panel. On day 10 post-operation, the inflammation response in both groups were clear with the formation of abundant irregular fibrous tissue; Right Panel. Twenty-eight days later, the boundary of the Mg-enriched allograft was already unable to be identified, and the implanted graft and host bone gradually become homogeneous (the dark blue dotted line highlights the allograft implanted and the red arrows indicate the cartilaginous-like tissue, stained red by F&S staining). (b) Histology of decellularized allografts, Mg-enriched (1hr) and Mg-enriched (4hr) allografts at 10 days post-op via SEM and the relative elemental composition list and mappings obtained using the EDS technique. The relative magnesium concentration of the defect implanted with Mg-enriched (4hr) graft is found to be higher. (For interpretation of the references to color in this figure legend, the reader is referred to the Web version of this article.)
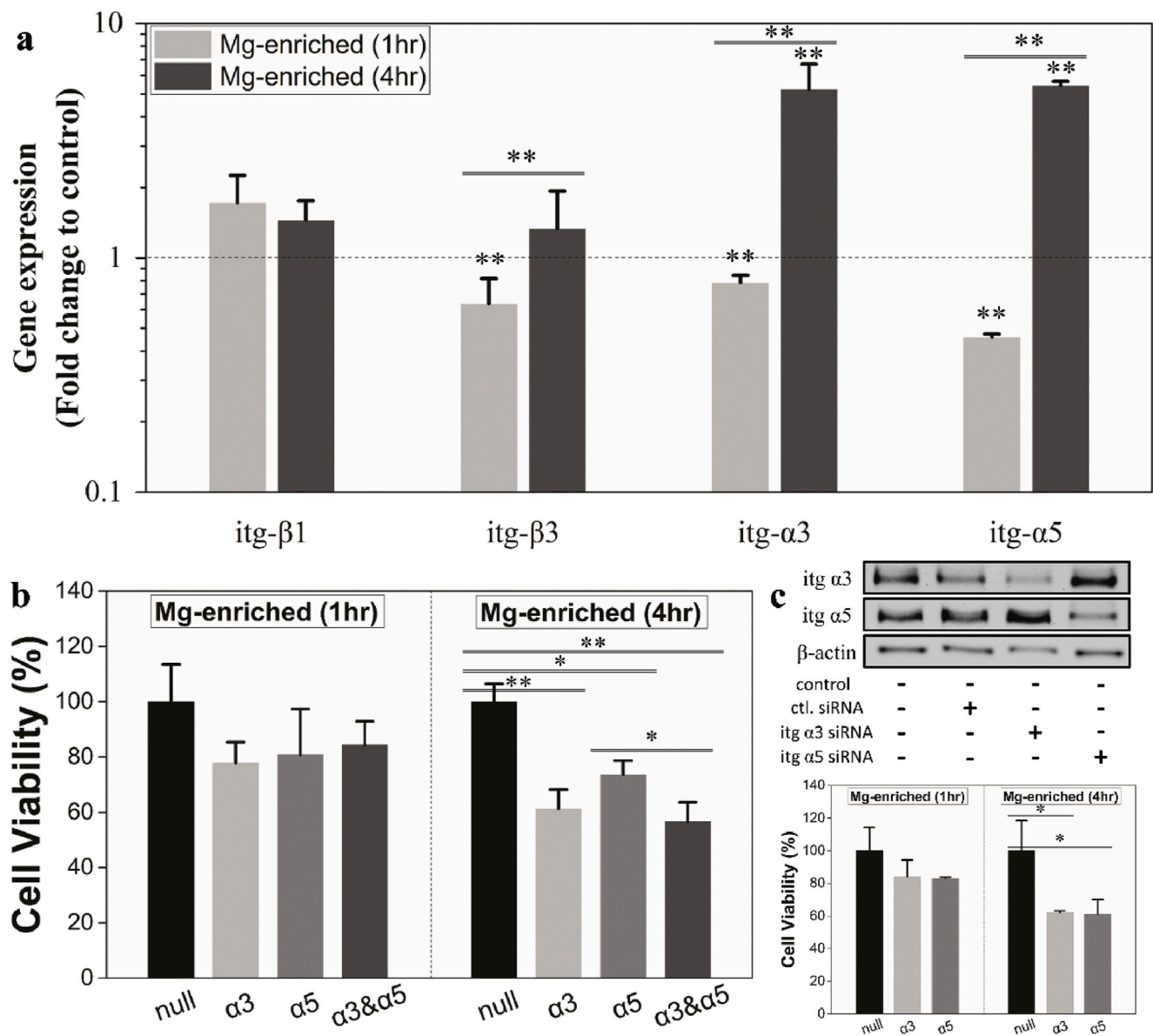
Fig. 8. Evaluation of integrin-mediated cell adhesion in the magnesium cationic cue enriched interfacial tissue microenvironment. (a) The mRNA expression level of several integrin receptor subunits detected from hTMSCs cultured with different samples for 24 h by RT-qPCR tests ($n = 5$). The mRNA levels for integrin α3 and α5 are significantly upregulated. (b) Inhibition of adhesion of hTMSCs to different samples after antibody-blocking treatments ($n = 3$). (c) Cell adhesion test of hTMSCs to different samples after siRNA treatments ($n = 3$). Data implied that the integrin-mediated cell adhesion was notable in the magnesium cationic cue enriched tissue microenvironment but not on the Mg-treated control samples. Error bars indicated means ± standard deviations. Statistically significance is indicated by *$p < 0.05$, **$p < 0.01$.

To further clarify whether the integrin subunits mediated cell adhesion on the surface of Mg-enriched (4hr) bone slices, the adherent cells after the antibody-blocking treatment or RNA interference were assayed using the MTT method. As illustrated in Fig. 8b, the cell viability, which indicates the number of adherent cells on the surface of different samples, was partially reduced after blocking either integrin α3 or α5 in the magnesium catioinic cue enriched interfacial tissue microenvironment over the surface of the Mg-enriched (4hr) graft, and the cell viability after blocking both integrin α3 and α5 was even lower. Nonetheless, decreased cell viability was not notable when cells were cultured on the Mg-enriched (1hr) samples after antibody blocking. This phenomenon was then verified using siRNA treatment. These results suggested that the adhesion of hTMSCs is mediated by the specific integrin subunits in the magnesium cationic cue enriched interfacial TME exerted by the Mg-enriched (4hr) graft.

4. Discussion

Osseointegration of a bone allograft to host bone is usually initiated by cellular attachment after the tissue inflammatory cascade [33]. Inferior cellular interaction in the interfacial tissue microenvironment and the absence of established mature bone at the interface may lead to insufficient bone allograft integration, resulting in poor patient recovery [34], which is not rare in gamma-irradiated allograft failure. Therefore, it is possible to alter the interfacial tissue microenvironment over the bone graft surface so as to facilitate healing of the gamma-irradiated allograft and osseointegration using a simple method, such as magnesium plasma treatment.

It has been documented that a proper cell/material interaction can be engineered in order to exert a fabourable extracellular tissue microenvironment (TME) for tissue regeneration [35]. Previous studies, such

as the bioresorbable implant [36,37], microsphere-based carrier [38, 39], and 3D-printed bone scaffold [20,40] had already demonstrated that the manipulated TME with spatiotemporal Mg^{2+} concentration accelerated bone regeneration. However, overdose of Mg^{2+} could be detrimental in terms of bone healing [41,42]. In this study, we were able to identify the significance of chemical cue in TME for bone regeneration. For instance, the Mg^{2+} concentration over the surface of bone graft analyzed by SIET was significantly higher than those measured from *in vitro* medium immersion (Fig. 3). This finding suggests that Mg cationic cue exerted on bone matrix surface is also sufficient to establish a proper TME in confined area that convinces effective bone regeneration.

The osseointegration of Mg-enriched and control allograft bones were compared in a well-established rodent model, which is analogous to the clinical use of allografts [10]. In the 28 days post-implantation, bone healing in the gamma-irradiated allograft group was predominated by creep substitution as indicated by the continuous bone resroption, whereas new bone formation was found along the Mg-enriched (4hr) allograft bone at post-operative day 10 (Fig. 6a). The subsequent EDS analysis on histological slides revealed that the allograft reinforced by magnesium cationic cue had a higher Mg content than the controls. A previous study has demonstrated that local enhancement of the magnesium level can suppress osteoclast formation and bone resorption *in vitro* [43]. This finding may help explain the discrepancy between our magnesium-enriched bone allografts and the controls *in vivo* with regard to bone formation and resorption. Directly after the inflammation, the MSCs recruitment and formation of a cartilaginous callus, which later undergoes mineralization and resorption and is replaced by bone, play a key feather in osseointegration [44,45]. As previously illustrated, magnesium was not only able to enhance adhesion, but also promoted the chondrogenesis of MSCs *in vitro*, and thus the formation of a cartilaginous callus in an animal model [46]. Therefore, we believe that the Mg cationic cue enriched tissue microenvironment contributed to the superior osseointegration in the Mg-enriched (4hr) bone allograft as it permits the bony ingrowth that leading to the homogeneous and accelerated bone regeneration in terms of distance osteogenesis and contact osetogenesis along the girder of allograft bone. Regarding the gamma-irradiated graft, the non-mineralized cartilaginous-like tissue was still identifiable in the control group even after implantion for 28 days (Fig. 7a), which is a typical symptom of distance osteogenesis and suggesting retarted bone-implant contact [33]. This speculation is confirmed by the analysis of the density of the non-mineralized tissue, which showed that the density was already restored at 21 days post-operation in the Mg-enriched (4hr) group but not in the control group (Fig. 6c).

The cellular responses in the magnesium cationic cue enriched interfacial tissue microenvironment were also systematically analyzed. Integrin-mediated signaling cascades, which were composed of α and β subunits, were found to play the key role in the modulation of cell attachment. For this research, the mRNA levels of several integrin subunits expressed by MSCs were analyzed (Fig. 8a), and the integrin α_3 and α_5 found on Mg-enriched (4hr) grafts were significantly upregulated after being cultured for 24 h. These integrin subunits were reported to be primarily responsible for cell adhesion [47], which is also strongly associated with the divalent cation, especially on Mg^{2+} and the Mg^{2+}/Ca^{2+} ratio [48]. By contrast, the adherent cells were significantly decreased in the same interfacial TME when the integrin α_3 and α_5 or both were blocked or silenced (Fig. 8b and c). It is evidented that the hTMSCs attempted to occupy more surface area on the Mg-enriched (4hr) bone graft than the surface of the controls *in vitro*. This observation can be explained by the increased cation-binding domains of integrin in the Mg^{2+}-cue enriched interfacal tissue microenvironment

over the bone surface compared to the surface with less Mg cationic cue [49]. Meanwhile, the increased Mg^{2+}/Ca^{2+} ratio was also found leading to enhanced cation-dependent morphological conformation change of adherent cells, and this is also thought to be one of the driving forces for cell spreading [48]. Additionally, the integrin α_3 expressed on the Mg-enriched (4hr) samples was significantly upregulated and this specific integrin subunit is highly associated with cell proliferation. It was reported that the knockdown of integrin α_3 led to a decreased proliferation of MSC, even though the cells were cultured in the Mg cation supplemented medium [50].

As a well-orchestrated process after initial attachment, the initial osteogenic response of the hTMSCs is also believed to be strongly associated with the upregulation of integrin subunits [51] and thus directly correlated to the early osseointegration responding to the allograft bone [8]. The ALP and Runx2 are the early osteogenic differentiation markers expressed by osteoblasts. Our findings not only demonstrated the up-regulation of the ALP and Runx2 genes when the cells were cultured in an Mg cationic cue enriched bone tissue microenvironment, but also promoted the early expression of extracellular matrix (ECM) marker, such as the Type I collagen (Colla1). Indeed, the correlations between the integrin subunits and osteogenic differentiation had been investigated by several groups [52,53]. Gain-of-function analysis found that integrin α_5 could promote the expression of osteoblast phenotypic markers (Runx2, ALP, and collagen type I) and the osteogenesis of hMSCs. These observations had been proven by the mediation of focal adhesion of ERK1/2-MAPKs and PI3K signalling pathways [54]. Subsequently, osteocalcin (OCN), which is an osteogenic differentiation marker in the later stage, was also elevated after 7 days of incubation in the Mg^{2+}-cue enriched interfacial tissue microenvironment. In fact, OCN is an osteoblast-specific non-collagenous bone ECM protein that involves in binding calcuim and hydroxyapatite [55]. The early expression of OCN supposed to induce effective mineral deposition *in vitro* (Fig. 5b) [56,57]. However, the OCN expression of Mg-enriched (4hr) sample in the culture of D21 did not differ to that of Mg-enriched (1hr) graft. Hence, we suspect that the early activation of mineralization and the higher calcium deposition rate may attribute to the upregulations of integrin subunits of MSCs under Mg^{2+}-cue enriched tissue microenvironment at early phase rather than the direct stimulation by the release of Mg^{2+}. In general, our findings suggest that a stable Mg cationic cue over the surface of bone allograft can establish a favorable interfacial tissue microenvironment that stimulates and orchestrates the expressions of integrin subunits of MSCs for subsequent early osseointegration.

Previous clinical study reported that the patients implanted with irradiated allografts demonstrated higher incidence of allograft fracture as compared with those without irradiation in the 5 years follow-up [58]. Indeed, the success of bone grafting surgery ultimately depends on the integration of bone graft with the host bone that provides sufficient mechanical support to the skeleton. A few studies had comprehensively investigated how gamma irradiation alter bone allograft in terms of mechanical properties, indicating that gamma irradiation procedure could compromise its mechanical integrity [12,59]. It is believed that the underlying cause is due to the fragmentation of collagen during irradiation. Additionally, gamma irradiation would alter the medullary lipids of bone allograft and therefore generate toxic compounds that directly jeopardized the functions of stem cells and other osteoprecursor cells [13,60]. Hence, the osseointegration capacity has been compromised. In our study, the customized plasma surface treatment would not cause any structural change in the collagen-like structure or compromise the mechanical properties of allograft bone after gamma irradiation (Fig. 1b, e), while the early ossteointegration
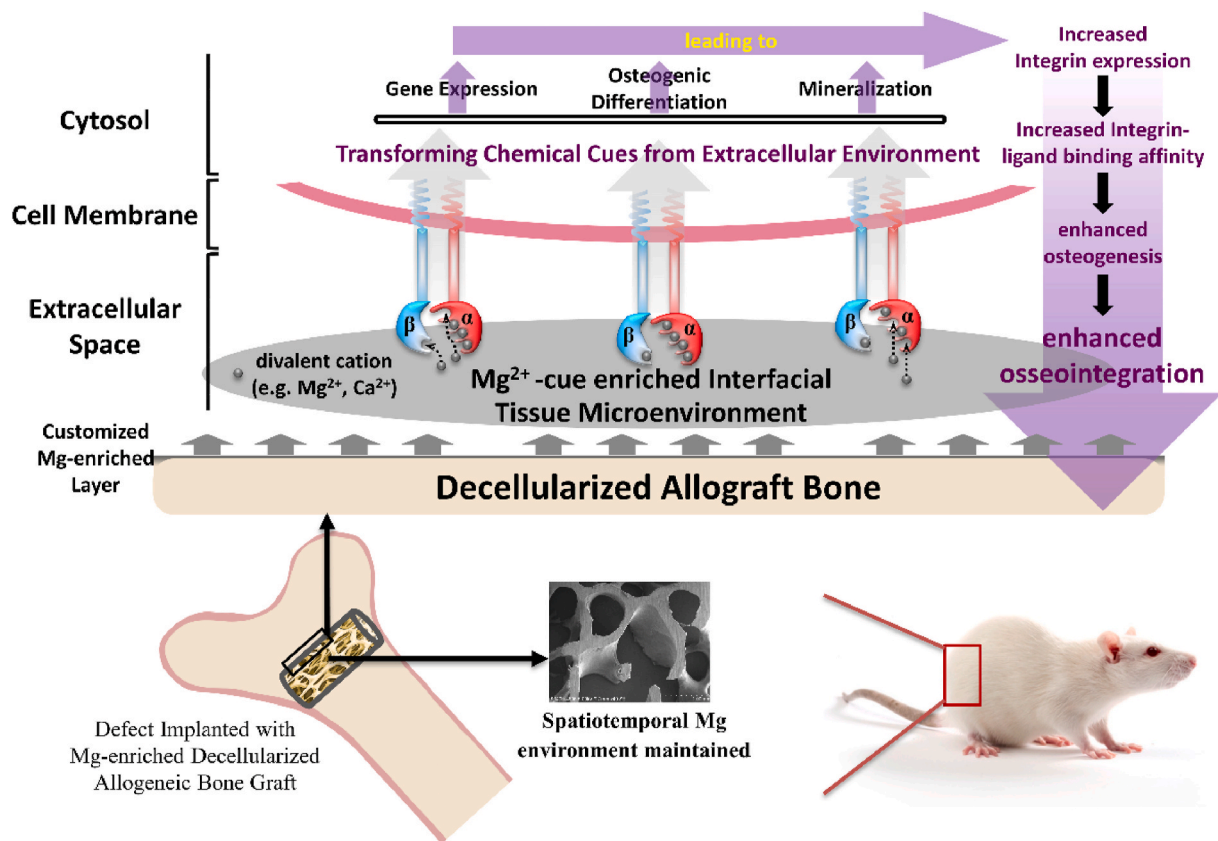
Fig. 9. Schematic illustration of the interaction of cells and magnesium cationic cue enriched interfacial tissue microenvironment over the surface of gamma-irradiated allograft bone and the orchestrated effect on osseointegration. The magnesium cationic cue enriched interfacial TME has been exerted on gamma-irradiated allograft bone without compromising the mechanical properties, and the ability of this interfacial tissue microenvironment to facilitate fracture healing and osseointegration has been recognized. More importantly, the up-regulation of integrin receptors induced by this interfacial tissue microenvironment is found to be pivotal for orchestrated cellular activity and promotes early osseointegration between the allograft and the host bone.

could be maintained. Hence, the current technique is unlikely to induce any such post-operative complications found in bone allograft augmentation surgery.

In summary, our *in vitro* and *in vivo* findings have revealed that the Mg cationic cue enriched interfacial tissue microenvironment is able to convince cell adhesion and spreading over allograft bone surface through the upregulation of several integrin receptors of MSCs, thereby elevating cell proliferation, osteogenic differentiation and mineralization, and finally leading to the enhanced bony ingrowth and the early osseointegration of allograft to the host bone. The interaction of cells and Mg cationic cue enriched interfacial tissue microenvironment is illustrated in Fig. 9.

5. Conclusion

An Mg cationic cue enriched interfacial tissue microenvironment was successfully established on the surface of allograft bone using a customized magnesium plasma treatment. This specifically treated allograft bone was able to maintain a fine-tuned interfacial TME over the surface of the Mg-enriched (4hr) allograft without compromising the mechanical properties of allograft bone. This interfacial tissue microenvironment was able to facilitate *in vitro* cell adhesion, proliferation and osteogenic differentiation, as well as new bone formation and osseointegration of the allograft to the host bone. These superior features were likely initiated by the upregulation of integrin α_3 and α_5 receptors of MSCs. Lastly, this study identifies a robust approach that can effectively enhance the bioactivity of a allograft bone and its subsequent osseointegration to a host bone without the aids of biological growth factors or stem cell therapy.

Author contributions

The manuscript was written through contributions of all authors. All authors have given approval to the final version of the manuscript. [1]These authors contributed equally.

Notes

The authors declare no competing financial interest.

CRediT authorship contribution statement

Wenhao Wang: Conceptualization, Data curation, Formal analysis, Investigation, Methodology, Validation, Visualization, Roles, Writing – original draft, Writing – review & editing. **Jie Shen:** Methodology, Funding acquisition, Validation, Visualization, Writing – review & editing. **Yuan Meng:** Methodology, Funding acquisition, Validation, Visualization, Writing – review & editing. **Miaoman Ye:** Investigation, Methodology, Validation, Visualization. **Shaozhang Lin:** Investigation, Methodology, Validation, Visualization. **Qi Zhao:** Investigation, Methodology, Validation, Visualization. **Le Wang:** Funding acquisition, Resources, Conceptualization, Methodology, Validation. **Kenneth M.C. Cheung:** Funding acquisition, Resources, Conceptualization, Methodology, Validation. **Shuilin Wu:** Funding acquisition, Resources, Conceptualization, Methodology, Validation. **Yufeng Zheng:** Funding acquisition, Resources, Conceptualization, Methodology, Validation. **Xuanyong Liu:** Funding acquisition, Resources, Conceptualization, Methodology, Validation. **Paul K. Chu:** Funding acquisition, Resources, Conceptualization, Methodology, Validation. **Kelvin W.K. Yeung:**

Conceptualization, Supervision, Funding acquisition. **Zhi-Yong Zhang:** Conceptualization, Supervision, Funding acquisition.

Declaration of competing interest

The authors declare that we have no financial and personal relationships with other people or organizations that can inappropriately influence our work, there is no professional or other personal interest of any nature or kind in any product, service and/or company that could be construed as influencing the position presented in the manuscript entitled "Magnesium Cationic Cue Enriched Interfacial Tissue Microenvironment Nurtures the Osseointegration of Gamma-irradiated Allograft Bone".

Acknowledgments

Appendix A. Supplementary data

Supplementary data to this article can be found online at https://doi.org/10.1016/j.bioactmat.2021.08.027.

References

[1] B.W. Schreurs, J. Luttjeboer, T.M. Thien, M.C. de Waal Malefijt, P. Buma, R. P. Veth, et al., Acetabular revision with impacted morselized cancellous bone graft and a cemented cup in patients with rheumatoid ArthritisA concise follow-up, at eight to nineteen years, of a previous report*, J. Bone Joint Surg. 91 (2009) 646–651.

[2] P.-L. Docquier, C. Delloye, Treatment of aneurysmal bone cysts by introduction of demineralized bone and autogenous bone marrow, J. Bone Joint Surg. 87 (2005) 2253–2258.

[3] P. Augat, U. Simon, A. Liedert, L. Claes, Mechanics and mechano-biology of fracture healing in normal and osteoporotic bone, Osteoporosis Int 16 (2005) S36–S43.

[4] P.V. Giannoudis, H. Dinopoulos, E. Tsiridis, Bone substitutes: an update, Injury 36 (2005) S20–S27.

[5] H. Shegarfi, O. Reikeras, Bone transplantation and immune response, J. Orthop. Surg. 17 (2009) 206–211.

[6] V. Campana, G. Milano, E. Pagano, M. Barba, C. Cicione, G. Salonna, et al., Bone substitutes in orthopaedic surgery: from basic science to clinical practice, J. Mater. Sci. Mater. Med. 25 (2014) 2445–2461.

[7] W.L. Murphy, T.C. McDevitt, A.J. Engler, Materials as stem cell regulators, Nat. Mater. 13 (2014) 547–557.

[8] S. Chen, Y. Guo, R. Liu, S. Wu, J. Fang, B. Huang, et al., Tuning surface properties of bone biomaterials to manipulate osteoblastic cell adhesion and the signaling pathways for the enhancement of early osseointegration, Colloids Surf. B Biointerfaces 164 (2018) 58–69.

[9] T.L. Sellaro, A.K. Ravindra, D.B. Stolz, S.F. Badylak, Maintenance of hepatic sinusoidal endothelial cell phenotype in vitro using organ-specific extracellular matrix scaffolds, Tissue Eng. 13 (2007) 2301–2310.

[10] N. Russell, R.A. Oliver, W.R. Walsh, The effect of sterilization methods on the osteoconductivity of allograft bone in a critical-sized bilateral tibial defect model in rabbits, Biomaterials 34 (2013) 8185–8194.

[11] D. Cohn Yakubovich, U. Eliav, E. Yalon, Y. Schary, D. Sheyn, G. Cook-Wiens, et al., Teriparatide attenuates scarring around murine cranial bone allograft via modulation of angiogenesis, Bone 97 (2017) 192–200.

[12] B. Burton, A. Gaspar, D. Josey, J. Tupy, M.D. Grynpas, T.L. Willett, Bone embrittlement and collagen modifications due to high-dose gamma-irradiation sterilization, Bone 61 (2014) 71–81.

[13] S.A. Lietman, W.W. Tomford, M.C. Gebhardt, D.S. Springfield, H.J. Mankin, Complications of irradiated allografts in orthopaedic tumor surgery, Clin. Orthop. Relat. Res. 375 (2000) 214–217.

[14] N. Reznikov, M. Bilton, L. Lari, M.M. Stevens, R. Kröger, Fractal-like hierarchical organization of bone begins at the nanoscale, Science (80) 360 (2018) eaao2189.

[15] M.J. Dalby, N. Gadegaard, R. Tare, A. Andar, M.O. Riehle, P. Herzyk, et al., The control of human mesenchymal cell differentiation using nanoscale symmetry and disorder, Nat. Mater. 6 (2007) 997–1003.

[16] A.J. Engler, S. Sen, H.L. Sweeney, D.E. Discher, Matrix elasticity directs stem cell lineage specification, Cell 126 (2006) 677.

[17] D.S. Benoit, M.P. Schwartz, A.R. Durney, K.S. Anseth, Small functional groups for controlled differentiation of hydrogel-encapsulated human mesenchymal stem cells, Nat. Mater. 7 (2008) 816–823.

[18] M.P. Lutolf, J.A. Hubbell, Synthetic biomaterials as instructive extracellular microenvironments for morphogenesis in tissue engineering, Nat. Biotechnol. 23 (2005) 47–55.

[19] M.D. Hoffman, C. Xie, X. Zhang, D.S. Benoit, The effect of mesenchymal stem cells delivered via hydrogel-based tissue engineered periosteum on bone allograft healing, Biomaterials 34 (2013) 8887–8898.

[20] X. Zhai, C. Ruan, Y. Ma, D. Cheng, M. Wu, W. Liu, et al., 3D-Bioprinted osteoblast-laden nanocomposite hydrogel constructs with induced microenvironments promote cell viability, differentiation, and osteogenesis both in vitro and in vivo, Advanced Science (2017) 1700550.

[21] J. Shen, B. Chen, X. Zhai, W. Qiao, S. Wu, X. Liu, et al., Stepwise 3D-spatio-temporal magnesium cationic niche: nanocomposite scaffold mediated microenvironment for modulating intramembranous ossification, Bioactive materials 6 (2021) 503–519.

[22] D. Laurencin, N. Almora-Barrios, N.H. de Leeuw, C. Gervais, C. Bonhomme, F. Mauri, et al., Magnesium incorporation into hydroxyapatite, Biomaterials 32 (2011) 1826–1837.

[23] W. Wang, H. Wong, F. Leung, K. Cheung, K. Yeung, Magnesium ions enriched decellularized bone allografts for bone tissue engineering, Tissue Eng Part A 21 (S1) (2015) S–232.

[24] Y. Zhao, D. Guo, S. Hou, H. Zhong, J. Yan, C. Zhang, et al., Porous allograft bone scaffolds: doping with strontium, PloS One 8 (2013), e69339.

[25] A. Dumas, C. Gaudin-Audrain, G. Mabilleau, P. Massin, L. Hubert, M.F. Basle, et al., The influence of processes for the purification of human bone allografts on the matrix surface and cytocompatibility, Biomaterials 27 (2006) 4204–4211.

[26] M.F. Moreau, Y. Gallois, M.-F. Baslé, D. Chappard, Gamma irradiation of human bone allografts alters medullary lipids and releases toxic compounds for osteoblast-like cells, Biomaterials 21 (2000) 369–376.

[27] S. Lamaka, O. Karavai, A. Bastos, M. Zheludkevich, M. Ferreira, Monitoring local spatial distribution of Mg 2+, pH and ionic currents, Electrochem. Commun. 10 (2008) 259–262.

[28] Y. Shen, W. Liu, K. Lin, H. Pan, B.W. Darvell, S. Peng, et al., Interfacial pH: a critical factor for osteoporotic bone regeneration, Langmuir 27 (2011) 2701–2708.

[29] K. Mihara, C. Imai, E. Coustan-Smith, J.S. Dome, M. Dominici, E. Vanin, et al., Development and functional characterization of human bone marrow mesenchymal cells immortalized by enforced expression of telomerase, Br. J. Haematol. 120 (2003) 846–849.

[30] K.L. Fung, R.H. Liang, G.C. Chan, Vincristine but not imatinib could suppress mesenchymal niche's support to lymphoid leukemic cells, Leuk. Lymphoma 51 (2010) 515–522.

[31] Y. Zhao, H.M. Wong, W. Wang, P. Li, Z. Xu, E.Y. Chong, et al., Cytocompatibility, osseointegration, and bioactivity of three-dimensional porous and nanostructured network on polyetheretherketone, Biomaterials 34 (2013) 9264–9277.

[32] Z. Lin, J. Wu, W. Qiao, Y. Zhao, K.H.M. Wong, P.K. Chu, et al., Precisely controlled delivery of magnesium ions thru sponge-like monodisperse PLGA/nano-MgO-alginate core-shell microsphere device to enable in-situ bone regeneration, Biomaterials 174 (2018) 1–16.

[33] F.A. Shah, P. Thomsen, A. Palmquist, Osseointegration and current interpretations of the bone-implant interface, Acta Biomater. 84 (2019) 1–15.

[34] H. Zreiqat, C. Howlett, A. Zannettino, P. Evans, G. Schulze-Tanzil, C. Knabe, et al., Mechanisms of magnesium-stimulated adhesion of osteoblastic cells to commonly used orthopaedic implants, J. Biomed. Mater. Res. 62 (2002) 175–184.

[35] J.J. Rice, M.M. Martino, L.L. De, F. Tortelli, P.S. Briquez, J.A. Hubbell, Engineering the regenerative microenvironment with biomaterials, Adv Healthc Mater 2 (2013) 57–71.

[36] T.A. Grunewald, H. Rennhofer, B. Hesse, M. Burghammer, S.E. Stanzl-Tschegg, M. Cotte, et al., Magnesium from bioresorbable implants: distribution and impact on the nano- and mineral structure of bone, Biomaterials 76 (2016) 250–260.

[37] Y. Zhang, J. Xu, Y.C. Ruan, M.K. Yu, M. O'Laughlin, H. Wise, et al., Implant-derived magnesium induces local neuronal production of CGRP to improve bone-fracture healing in rats, Nat. Med. 22 (2016) 1160–1169.

[38] S. Lin, G. Yang, F. Jiang, M. Zhou, S. Yin, Y. Tang, et al., A magnesium-enriched 3D culture system that mimics the bone development microenvironment for vascularized bone regeneration, Adv. Sci. 6 (2019) 1900209.

[39] Z. Lin, D. Shen, W. Zhou, Y. Zheng, T. Kong, X. Liu, et al., Regulation of extracellular bioactive cations in bone tissue microenvironment induces favorable osteoimmune conditions to accelerate in situ bone regeneration, Bioactive materials 6 (2021) 2315–2330.

[40] J. Shen, W. Wang, X. Zhai, B. Chen, W. Qiao, W. Li, et al., 3D-printed nanocomposite scaffolds with tunable magnesium ionic microenvironment induce in situ bone tissue regeneration, Applied Materials Today 16 (2019) 493–507.

[41] J.F. Navarro-González, C. Mora-Fernández, J. García-Pérez, Reviews: Clinical Implications of Disordered Magnesium Homeostasis in Chronic Renal Failure and Dialysis, Semin Dial: Wiley Online Library, 2009, pp. 37–44.

[42] J. Shen, B. Chen, X. Zhai, W. Qiao, S. Wu, X. Liu, et al., Stepwise 3D-spatio-temporal magnesium cationic niche: nanocomposite scaffold mediated microenvironment for modulating intramembranous ossification, Bioactive materials 6 (2021) 503–519.

[43] Z. Zhai, X. Qu, H. Li, K. Yang, P. Wan, L. Tan, et al., The effect of metallic magnesium degradation products on osteoclast-induced osteolysis and attenuation of NF-kappaB and NFATc1 signaling, Biomaterials 35 (2014) 6299–6310.

[44] R. Marsell, T.A. Einhorn, The biology of fracture healing, Injury 42 (2011) 551–555.

[45] T.A. Einhorn, L.C. Gerstenfeld, Fracture healing: mechanisms and interventions, Nat. Rev. Rheumatol. 11 (2015) 45–54.

[46] M. Shimaya, T. Muneta, S. Ichinose, K. Tsuji, I. Sekiya, Magnesium enhances adherence and cartilage formation of synovial mesenchymal stem cells through integrins, Osteoarthritis Cartilage 18 (2010) 1300–1309.

[47] J.E. Frith, R.J. Mills, J.E. Hudson, J.J. Cooper-White, Tailored integrin-extracellular matrix interactions to direct human mesenchymal stem cell differentiation, Stem Cells Dev 21 (2012) 2442–2456.

[48] J.J. Grzesiak, G.E. Davis, D. Kirchhofer, M.D. Pierschbacher, Regulation of alpha 2 beta 1-mediated fibroblast migration on type I collagen by shifts in the concentrations of extracellular Mg2+ and Ca2+, JCB (J. Cell Biol.) 117 (1992) 1109.

[49] J.-P. Declercq, B. Tinant, J. Parello, J. Rambaud, Ionic interactions with parvalbumins: crystal structure determination of pike 4.10 parvalbumin in four different ionic environments, J. Mol. Biol. 220 (1991) 1017–1039.

[50] Y.H. Leem, K.S. Lee, J.H. Kim, H.K. Seok, J.S. Chang, D.H. Lee, Magnesium ions facilitate integrin alpha 2- and alpha 3-mediated proliferation and enhance alkaline phosphatase expression and activity in hBMSCs, J Tissue Eng Regen Med 10 (2016) E527–E536.

[51] S.L. Cheng, C.F. Lai, A. Fausto, M. Chellaiah, X. Feng, K.P. McHugh, et al., Regulation of αVβ3 and αVβ5 integrins by dexamethasone in normal human osteoblastic cells, J. Cell. Biochem. 77 (2000) 265–276.

[52] M.M. Martino, M. Mochizuki, D.A. Rothenfluh, S.A. Rempel, J.A. Hubbell, T. H. Barker, Controlling integrin specificity and stem cell differentiation in 2D and 3D environments through regulation of fibronectin domain stability, Biomaterials 30 (2009) 1089–1097.

[53] Y.K. Wang, C.S. Chen, Cell adhesion and mechanical stimulation in the regulation of mesenchymal stem cell differentiation, J. Cell Mol. Med. 17 (2013) 823–832.

[54] Z. Hamidouche, O. Fromigue, J. Ringe, T. Haupl, P. Vaudin, J.C. Pages, et al., Priming integrin alpha5 promotes human mesenchymal stromal cell osteoblast differentiation and osteogenesis, Proc. Natl. Acad. Sci. U. S. A. 106 (2009) 18587–18591.

[55] C. Granéli, A. Thorfve, U. Ruetschi, H. Brisby, P. Thomsen, A. Lindahl, et al., Novel markers of osteogenic and adipogenic differentiation of human bone marrow stromal cells identified using a quantitative proteomics approach, Stem Cell Res. 12 (2014) 153–165.

[56] S. Yoshizawa, A. Brown, A. Barchowsky, C. Sfeir, Role of magnesium ions on osteogenic response in bone marrow stromal cells, Connect. Tissue Res. 55 (Suppl 1) (2014) 155–159.

[57] S. Yoshizawa, A. Brown, A. Barchowsky, C. Sfeir, Magnesium ion stimulation of bone marrow stromal cells enhances osteogenic activity, simulating the effect of magnesium alloy degradation, Acta Biomater. 10 (2014) 2834–2842.

[58] S.A. Lietman, W.W. Tomford, M.C. Gebhardt, D.S. Springfield, H.J. Mankin, Complications of irradiated allografts in orthopaedic tumor surgery, Clin. Orthop. Relat. Res. 375 (2000) 214–217.

[59] N.A. Russell, M.H. Pelletier, W.J. Bruce, W.R. Walsh, The effect of gamma irradiation on the anisotropy of bovine cortical bone, Med. Eng. Phys. 34 (2012) 1117–1122.

[60] B. Han, Z. Yang, M. Nimni, Effects of gamma irradiation on osteoinduction associated with demineralized bone matrix, J. Orthop. Res. 26 (2008) 75–82.